International Journal of Biological Macromolecules 260 (2024) 129496

Contents lists available at ScienceDirect

International Journal of Biological Macromolecules

journal homepage: www.elsevier.com/locate/ijbiomac

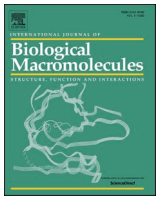

Matrix hyaluronic acid and bilayer poly-hydroxyethyl methacrylate-hyaluronic acid films as potential ocular drug delivery platforms

Mohammad Tighsazzadeh, Joshua Boateng *

School of Science, Faculty of Engineering and Science, University of Greenwich, Medway, Kent ME4 4TB, UK

ARTICLE INFO

Keywords:
EpiCorneal™
Glaucoma
Hyaluronic acid
Porcine cornea
Poly-hydroxyethyl methacrylate
Timolol

ABSTRACT

This study aimed to design hydrogel based films comprising hyaluronic acid (HA) to overcome limitations of currently used eye drops. Timolol-loaded crosslinked (X2) HA-based and bilayer (B2) (pHEMA/PVP-HA-based layers) films were designed and characterized. The films were transparent (UV, visual observation) with cross-linked (<80 %) films showing lower light transmittance than bilayer (>80 %) films. X2 showed significantly higher swelling capacity, tensile strength and elastic modulus (5491.6 %, 1539.8 Nmm^{-2}, 1777.2 mPa) than B2 (1905.0 %, 170.0N mm^{-2}, 67.3 mPa) respectively. However, X2 showed lower cumulative drug released and adhesive force (27.3 %, 6.2 N) than B2 (57.5 %, 8.6 N). UV sterilization did not significantly alter physical properties, while SEM and IR microscopy showed smooth surface morphology and homogeneous drug distribution. Timolol permeation (EpiCorneal™/porcine cornea) depended on the film matrix with erodible films showing similar permeation to commercial eyedrops. Drug permeation for porcine cornea (X2 = 549.0.2, B2 = 312.1 $\mu gcm^{-2}\ h^{-1}$) was significantly faster than EpiCorneal™ (X2 = 55.2, B2 = 37.6 $\mu gcm^{-2}\ h^{-1}$), but with a linear correlation between them. All the selected optimized films showed acceptable compatibility (MTT assay) with both HeLa cells and EpiCorneal™. In conclusion, crosslinked and bilayer HA based films showed ideal characteristics suitable for potential ocular drug delivery, though further work is required to further optimize these properties and confirm their efficacy including *in vivo* tests.

1. Introduction

Ocular diseases and impairments such as age-related macular degeneration (AMD), diabetic retinopathy, cataract, and glaucoma affect the quality of life of numerous people globally. The number of visually impaired people was estimated to be 553 (295 moderate and severe, and 258 mild) million worldwide with associated social and economic burdens [1]. The anatomy and physiology of the eye present a huge challenge for drug delivery including the need to directly administer drugs to ocular tissues to avoid systemic exposure and consequent side effects. Delivering therapeutic agents to specific intraocular targets and achieving optimal drug concentration is limited by a number of inherent anatomical and physiological barriers. These include the cornea, anterior segment barriers, sclera and Bruch's-choroid complex as well as the blood-retinal barrier. These natural barriers not only protect the eye from invasion by foreign substances but also regulate the milieu of intraocular tissues, which is essential for maintaining ocular physiological function [2]. These tight barriers limit the diffusion and penetration of ophthalmic agents.

One of the most common dosage forms used to manage intraocular diseases is eye drops. However, eye drops are limited by their low bioavailability with only 5–10 % of the administered dose reaching the target tissue. Other traditional formulations include gels [3] and ointments [4] which remain longer on the eye, however, like eye drops, gels and ointments eventually become diluted with tear fluid and are also subsequently displaced through blinking and drainage. In the past decade, novel therapies have been developed to overcome these limitations by improving drug residence times on the cornea. These include nanoparticles [5], liposomes [6], microemulsions [7], nanosuspensions [8], polymeric micelles [9,10], biodegradable microneedles [11,12] and hydrogel-based delivery systems.

The use of hydrogels in ophthalmic applications is well established and has been applied in various forms such as contact lenses [13], *in-situ* gelling systems [14] and implants [15]. The most commonly used ocular

* Corresponding author.
E-mail address: j.s.boateng@gre.ac.uk (J. Boateng).

https://doi.org/10.1016/j.ijbiomac.2024.129496
Received 13 October 2023; Received in revised form 1 January 2024; Accepted 12 January 2024
Available online 18 January 2024

hydrogels are soft contact lenses (SCLs) which are used by millions of patients for vision correction and cosmetic purposes. The high patient acceptance of this topical device has made SCLs and thin films promising platforms for ocular drug delivery in chronic eye diseases such as glaucoma, where prolonged drug retention is necessary. This makes them a cheaper alternative to the other advanced systems proposed such as nanoparticles, liposomes, microemulsions, nanosuspensions, polymeric micelles and microneedles. The common polymers used for preparation of SCLs are (i) poly-hydroxyethyl methacrylate (pHEMA) and (ii) silicone with the latter showing increased popularity due to excellent oxygen penetration ability which allows patients to wear the SCLs for longer periods of time [16,17]. However, for research purposes, pHEMA-based hydrogels are more commonly used due to lower costs and easy access worldwide.

Many studies have used pHEMA-based hydrogels to investigate topical delivery of ocular drugs and their potential benefits over eye drops [18,19]. Most of these attempts have focused on soaking the dry hydrogel film in a drug solution until saturation. In this method, the amount of drug absorbed depends on its solubility, conformation, molecular weight, interaction with the hydrogel polymer, concentration and degree of swelling of the hydrogel in the drug solution [20]. Major limitations of drug-soaked hydrogels are the diffusion of water into the polymer and poor aqueous solubility of most drugs, resulting in very low uptake by the SCL which subsequently results in rapid release [21]. In addition, it takes a few hours to load the lens with the drug by diffusion (Fick's law) from the aqueous solution, and the large fraction of the drug that is left in the solution is wasted. Torres-Luna and colleagues investigated the use of cationic surfactants for controlling the release of diclofenac from pHEMA hydrogel contact lenses [22]. In a similar study, Lee and co-workers investigated drug delivery through pHEMA hydrogel contact lenses co-loaded with lipophilic vitamins [23]. Despite successful preparation of transparent hydrogels in both studies, the release profiles revealed that maximum drug release was achieved within only 4 h. Therefore, prolonged drug release was not achieved and this study seeks to increase the duration of drug release after application to reduce the need for too frequent administrations.

In the past decade, crosslinked hyaluronic acid (HA) based hydrogels and ocular inserts have been studied as potential topical delivery systems for ophthalmic drugs [24–26]. In a study by Calles and colleagues, crosslinked HA inserts were developed and loaded with timolol (TM) which demonstrated positive results in reducing intraocular pressure [24]. However, the inserts were not transparent and were placed in the cul de sac of the eye. In addition, the thickness of the optimum formulation (selected for *in vivo* studies) in their study was 300 μm which is above the maximum recommended thickness value (90 μm) of SCLs reported by Johnson & Johnson. In a follow up study by the same research group [25], the optimum formulation comprising HA crosslinked with poly(propylene glycol) diglycidyl ether (PEGDE) was further optimized to achieve transparent films. However, the films' thickness (157 μm) remained above the recommended 90 μm, and the drug release profiles and mechanisms were also not determined. In an interesting study, Korogiannaki and colleagues [27] investigated the release of TM from HA-containing silicone hydrogel contact lens materials. Despite incorporation of HA and PVP during synthesis of the contact lenses, maximum cumulative drug release was achieved in <3 h implying low drug retention. Successful topical delivery of drugs to the eye relies on effective diffusion of the drug molecules across the lipophilic and hydrophilic layers of the cornea. Strategies include prolonging residence times of the drug using viscosity enhancing (mucoadhesive) agents and *in situ* gels, employing penetration enhancers and colloidal systems (*e.g.* nanoparticles and liposomes).

Several animal eye models, including rabbit [28–31], rat [32], mouse [33,34], cat [35], dog [36,37] and pig [38–40] have been used to investigate topical delivery of ophthalmic drugs. Although *in vivo* studies are useful to study the efficacy of delivery systems, they are expensive to run and present ethical issues including concerns around animal welfare. *Ex vivo* experiments are less expensive and can be used to study drug permeation across the cornea with the pig eye considered a suitable model as it is very similar to the human eye with respect to size, vascular anatomy, histology, corneal thickness, and presence of Bowman's layer. Furthermore, with pigs being commonly used in human meat consumption, porcine ocular bulbs are easy to obtain from local slaughterhouses without any ethical concerns [41]. Though rabbit eyes are popular for *in vivo* studies due to easy *ex vivo–in vivo* correlation [42], they are smaller than human eyes, possess a nictitating membrane and have very low blinking frequency and higher permeability [43]. The recent development and commercialization of EpiOcular™ and EpiCorneal™ 3D human tissue models (MatTek Corporation, Ashland, MA, USA) provided a highly predictive non-animal alternative to evaluate ophthalmic drug delivery systems. Their reasonable cost, ready availability and ease of use have made these 3D tissues popular and reliable *in vitro* models for various areas of research such as buccal [44,45] and ocular [46,47] drug delivery.

Based on the current challenges with ocular drug delivery outlined above, this study aimed to design thin films that enhance the pre-corneal residence time, control release of the drug from the thin film matrices, and ultimately improve drug absorption for potential treatment of glaucoma. It will be beneficial to reduce the dose, dosing frequency and consequently, reduce potential side effects of drugs applied directly onto the eyes. We hypothesize that polysaccharide-based films in the form of (i) matrix crosslinked HA hydrogels or (ii) HA in combination with soft contact lens hydrogel materials *i.e.* pHEMA (bilayer film), represent suitable platforms for delivering drugs directly to the eye and overcome the limitations of currently used eye drops. This study reports on the formulation design and comparison of the functional physical and biological characteristics of different HA based ocular films (crosslinked HA and bilayer films) for delivering TM to potentially treat glaucoma. Finally, mechanical and physicochemical properties of these formulations were compared with erodible HA/HPMC-based matrix films previously reported [48]. In the case of the bilayer films, the drug was embedded directly into the HA layer to avoid the need for soaking the pHEMA hydrogel in drug solution which has many limitations as outlined above. The ultimate rationale was to improve retention time, prolong the release of drug, and in the case of the bilayer films, to achieve one directional release of the drug. To the best of our knowledge, this is the first study that compares the functional characteristics of TM loaded crosslinked HA films with bilayer films comprising TM loaded erodible HA layer and pHEMA hydrogel (contact lens) layer for the potential treatment of glaucoma. In addition, no study exists in the literature that tests permeation of TM released from HA-based films through EpiCorneal™ tissue (*in vitro*) and subsequently correlates the *in vitro* permeation with (*ex vivo*) permeation through pig cornea.

2. Materials and methods

2.1. Materials

Hydroxypropyl methylcellulose (HPMC) (1261.45 g/mol molecular weight and viscosity 4000 cP in water), timolol maleate (TM), poly (vinylpyrrolidone) (PVP), ethylene glycol dimethacrylate (EGDMA), itaconic acid (IT), poly(ethylene glycol) diglycidyl ether (PEGDE), 2-hydroxyethyl methacrylate (HEMA), Triton X-100, PBS tablets (pH 7.4), Krebs-Ringer bicarbonate buffer and 2,20-azobis(2-methylpropionitrile) (AIBN) were purchased from Sigma Aldrich, (Gillingham, UK). Glycerol (GLY), sodium bicarbonate, potassium chloride, calcium chloride, sodium chloride, mucin, glucose, Dulbecco's Modified Eagle's Medium, fetal bovine serum, penicillin-streptomycin, (3-(4,5-dimethylthiazol-2-yl)-2,5-diphenyltetrazolium bromide) (MTT) reagent and dimethyl sulfoxide (DMSO) were all purchased from Fisher Scientific, (Loughborough, UK). Hyaluronic acid (HA) (molecular weight 2.6×10^6) was purchased from Wisapple, (Beijing, China). EpiCorneal™ tissue kit (COR-100) was purchased from MatTek Corporation, (Ashland MA,

USA) and pig eyes were obtained from a local slaughterhouse (Tunbridge Wells, Kent, UK).

2.2. Preparation of ocular films

2.2.1. Composite films

Composite erodible films were prepared using solvent casting method as previously reported [48]. Briefly, TM was first dissolved in water prior to the addition of primary polymers (HA and HPMC) in a 1:1 ratio and plasticizer (GLY) with a total polymer to plasticizer ratio of 2:1.

2.2.2. Bilayer films

Bilayer films were prepared by adding a pHEMA/PVP hydrogel slurry on top of selected erodible films (blank or drug loaded-DL) prepared from 1 % w/v (HPMC only, composite HA/HPMC or HA only) gels plasticized with GLY, with the latter (HA only) selected for drug loading. The DL HA films contained TM (0.75 %) based on the total solid polymer content. To prepare pHEMA/PVP hydrogel (98/2, w/w), an appropriate amount of EGDMA (crosslinker) was dissolved in HEMA (hydrophilic monomer) to obtain an EGDMA concentration of 80 mM (Table 1). The resulting mixture was then degassed by sonication for 5 min and a gentle stream of nitrogen bubbled through it for 15 min before the addition of AIBN (10 mM) as initiator and PVP (0.02 g mL^{-1}). The mixture was stirred continuously for approximately 2 h on a magnetic stirrer to allow complete dissolution of PVP. The PVP acted as copolymer to produce crosslinked structures, comprising pHEMA blocks grafted onto a PVP matrix. Its main function was to increase wettability and moisture retention due to its hydrophilic property [49]. The completion of the polymerization reaction (Fig. 1a) was achieved at 50 °C over 14 h. The resulting hydrogels were washed over 5 days with twice deionized water (renewed three times a day) to remove unreacted monomers and to facilitate easy handling [50]. Finally, 10 g of the hydrated pHEMA/PVP slurry was poured on top of the previously prepared HA films (both blank and DL) and placed in 40 °C oven for 72 h to obtain dry bilayer films.

2.2.3. Crosslinked HA films

The crosslinked HA films were prepared as previously reported by Calles and co-workers [24,25] and illustrated in Fig. 1b, based on the formula in Table 1. TM-loaded crosslinked HA films were prepared by incorporating the appropriate amount of TM into 2 % w/w HA solution, using twice distilled water as solvent. The amount of each constituent was adjusted to produce 1:1:2 M ratios for HA:IT:PEGDE. IT provided an adequate acidic environment required for ionization of HA and subsequent crosslinking of the polymer chains by PEGDE. After 24 h reaction time (Fig. 1b) under slight stirring at room temperature, 35 g of the final gel was poured into a Petri dish and dried overnight in a vacuum oven at 40 °C. The various formulations prepared using different approaches were functionally characterized and compared, and the selected optimized DL films are summarized in Table 2.

Table 1
Formulation composition for blank and TM-loaded crosslinked (X) HA and bilayer (B) pHEMA/PVP-HA films[#]. X1 is blank crosslinked HA films, X2 is DL crosslinked HA films, B1 is blank pHEMA/PVP-HA bi-layer films, B2 is DL pHEMA/PVP-HA bilayer films.

Component	Function	X1 (mg)	X2 (mg)	B1 (mg)	B2 (mg)
HA	Film forming polymer	2000.0	2000.0	1000.0	1000.0
PEGDE	Crosslinker to HA	1.4	1.4	–	–
IT	Acidic catalyst for HA crosslinking	0.1	0.1	–	–
GLY	Plasticizer	125.0	125.0	500.0	500.0
AIBN	Reaction initiator during crosslinking of HEMA	–	–	165.0	165.0
EDGMA	Crosslinker for HEMA	–	–	165.0	165.0
HEMA	Monomer for preparing pHEMA hydrogel	–	–	98,000.0	98,000.0
PVP	Copolymer to HEMA in synthesis of pHEMA hydrogel	–	–	2000.0	2000.0
TM	Model glaucoma drug	–	15.0	–	7.5

2.3. Sterilization

The films were sterilized by exposing them to UV-C (short wave) radiation [51] with wavelength range of 280–200 nm over 24 h. Furthermore, to evaluate the potential deleterious effects of UV radiation, the films were evaluated for their tensile and mucoadhesive properties using a texture analyzer (details below) before and after sterilization and the results compared (n = 3).

2.4. Physical evaluation

2.4.1. Transparency

The transparency and clarity of the films were evaluated to ensure non-interference with sight upon application as previously reported [48,52]. Briefly the films were tested *via*; (i) qualitative measurement which involved placing the films over a marked ruler and determining ease of reading the markings and a digital image captured as evidence, (ii) semi-quantitative measurement through observation and scoring for transparency using adult human volunteers (scores ranged from 1 to 5 with 1 being completely transparent and 5 being completely opaque) and (iii) quantitatively measuring light transmission at wavelengths ranging from 290 to 700 nm using a UV spectrophotometer [53].

2.4.2. Weight, thickness, surface pH and folding endurance

The weight and thickness of the films were measured using an analytical balance and a micrometer screw gauge respectively [48]. Surface pH was measured for the hydrated films using a pH meter as previously reported [54]. Briefly, the films were placed in a Petri dish containing 100 mL of twice-distilled water (room temperature), covered and left to hydrate for 30 min. The hydrated film was placed in close contact with a digital pH meter and the surface pH recorded. The folding endurance was evaluated by repeated folding of the film at the same position at an angle of 180° until they broke or reached 300 folds as previously reported [55,56].

2.5. Swelling capacity

The swelling profiles of the films were measured using simulated tear fluid (STF) at pH 7.4 and temperature of 37 °C and prepared based on the formula shown in Table 3. The samples (n = 3) were cut into 35 mm diameter circular strips, accurately weighed (W_0) and placed in a Petri dish. An aliquot (2 mL) of STF was poured onto the weighed film to initiate hydration and swelling.

At regular time intervals, The STF was blotted out carefully using tissue paper and the weight of the swollen film (W_1) recorded. A further 2 mL of STF was placed on the swollen film and the entire process repeated till the films started to erode or disintegrate and the swelling capacity at each time point calculated using Eq. (1).

$$Swelling\ capacity = \left[\frac{(W_1 - W_0)}{W_0}\right] \times 100 \quad (1)$$

2.6. Texture analysis

Texture analysis was performed on the films to characterize their tensile and adhesive properties with the help of a texture analyzer

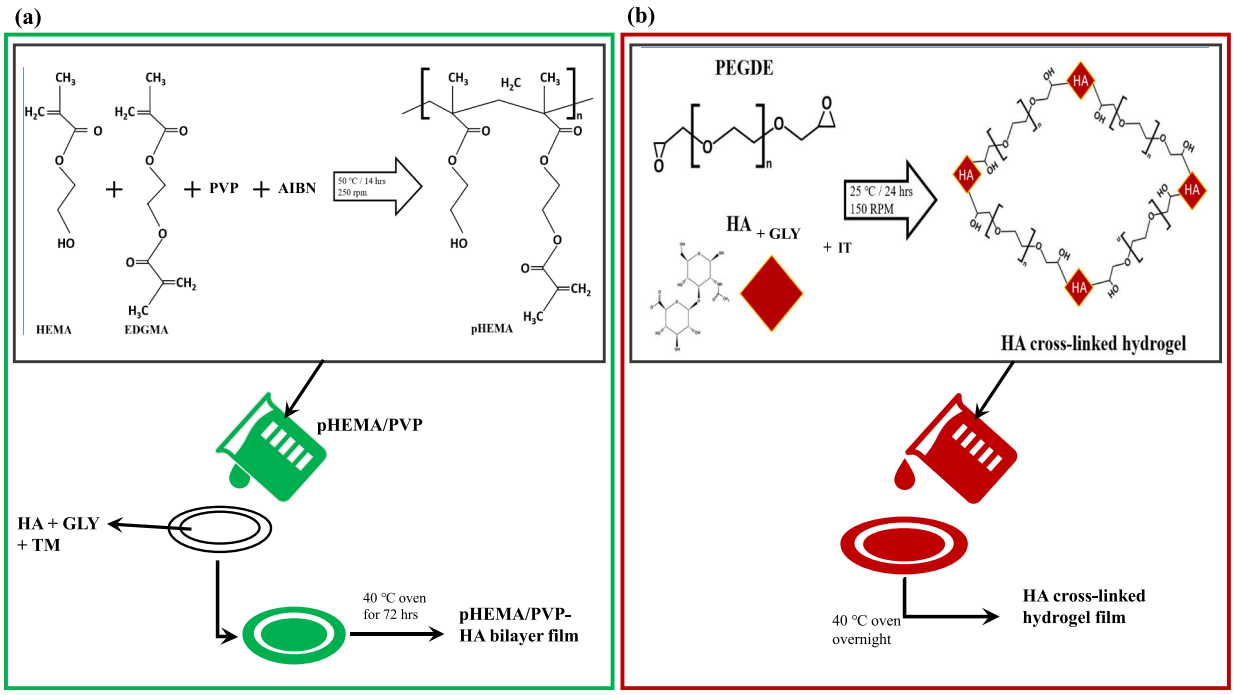

Fig. 1. (a) Polymerization of HEMA monomer to pHEMA using EDGMA as crosslinker in the presence of PVP co-polymer. The synthesized pHEMA/PVP hydrogel was then poured onto previously prepared HA films with or without TM and dried in an oven to obtain the bilayer films (b) crosslinking of HA polymer chains by PEGDE in the presence of IT. The crosslinked HA hydrogels with or without drug were then dried in an oven to obtain the crosslinked HA films.

Table 2
Composition for three selected optimized TM loaded formulations whose performance characteristics were compared: F3 - composite HA/HPMC films (reproduced from [48] with permission); X2 - crosslinked HA films; B2 - bilayer pHEMA/PVP-HA films. In the case of F3 the amount of HA (compared to that in B2) was reduced by 500 mg and replaced with the same amount of HPMC.

	F3 (mg)	B2 (mg)	X2 (mg)
HA	500.0	1000.0	2000.0
HPMC	500.0	–	–
PEGDE	–	–	1.4
IT	–	–	0.1
GLY	500.0	500.0	125.0
AIBN	–	165.0	–
EDGMA	–	165.0	–
HEMA	–	98,000.0	–
PVP	–	2000.0	–
TM	7.5	7.5	15.0

#Preliminary development work was undertaken by using different combinations (amounts) of film components to achieve formulations that were easily removable from the casting containers without being damaged and easy to handle. Based on these, three different types of film formulations were prepared for testing and their properties compared. As a result, the compositions of HA and GLY in the synthesized films differed for F3, X1/X2 and B1/B2. Further, the amount of TM present in the DL films was based on how much HA (X2, B2) and HA/HPMC (F3) to ensure the same percentage drug loading (0.75 %).

Table 3
Preparation of STF in 1 L of 2× deionized water.

Composition (in water)	Weight (g)
Sodium bicarbonate	0.1924
Potassium chloride	0.1111
Calcium chloride	0.0023
Sodium chloride	0.6728
Mucin	0.6690
Glucose	0.0025

(Stable Micro Systems, Surrey, UK).

2.6.1. Tensile properties

Dumb-bell shaped strips of each formulation (n = 3) were stretched between the tensile grips of the texture analyzer in tensile mode till they broke. The following instrument settings were applied: gauge length of 30 mm, 5 kg load cell, trigger force of 0.01 N, pre-test speed and the test speed were set at 1 mm s^{-1}, and post-test speed at 10 mm s^{-1}. Eqs. (2)–(4) were used to calculate the tensile strength, elastic modulus and percentage elongation respectively of each film from the force - time plots.

$$Tensile\ Strength = \frac{Force\ at\ Failure}{Cross - Sectional\ Area} \quad (2)$$

$$Elastic\ Modulus = \frac{Slope}{Crosshead\ Speed \times Cross - Sectional\ Area} \quad (3)$$

$$Percentage\ Elongation = \frac{Increase\ in\ Length\ (elongation)}{Original\ Length} \times 100 \quad (4)$$

2.6.2. In vitro mucoadhesion

Adhesive properties were evaluated using a 35 mm cylindrical probe with a 5 kg load cell against gelatin gel (20 g, 6.67 % w/v) which had been allowed to set. To simulate ocular mucosa environment, the gelatin gel was equilibrated with 500 μL of STF. The basis of the mucoadhesive test was the interaction between the films and mucin present in tear fluid. The gelatine gel was used to provide a solid support (mimicking the soft cornea) for the STF [48,57]. The films (n = 3) were cut into circular discs (35 mm in diameter), attached to the cylindrical probe and the probe programmed to approach the gelatin gel equilibrated with STF. The film was left in contact with the moist gelatin surface for 60 s to ensure complete contact, and subsequently withdrawn using a speed of 1 mm min^{-1} and 0.01 N trigger force until complete detachment from the gelatin gel. In the case of the bilayer films, the HA side was in direct contact with the model mucosa surface. The plotted mucoadhesion profiles were used to calculate the peak adhesive force (PAF), total work

of adhesion (TWA) representing the area under the force-distance curves and cohesiveness (distance travelled by probe before detachment) of the films.

2.7. Analytical characterization

Various analytical techniques including attenuated total reflectance Fourier transform infrared (ATR-FTIR) spectroscopy, X-ray diffraction (XRD) and thermal analyses were employed to characterize the different film formulations as well as the starting materials.

For the ATR-FTIR analysis, a Perkin Elmer Two ATR-FTIR spectrophotometer (Seer Green, UK) was used at a wavenumber range of 450 to 4000 cm^{-1} with resolution of 32 cm^{-1} and scan speed of 0.2 cm^{-1}. For XRD analysis, diffractograms were obtained in transmission mode with the help of a Bruker diffractometer equipped with a DIFFRAC plus XRD Commander from 2θ range of 5°- 50° and the following instrument settings were applied; step size (0.04°), scan speed (0.2 s/step), voltage (40 kV) and current (40 mA) with Cu Kα radiation.

Thermal analyses were undertaken using thermogravimetric analysis (TGA) and modulated differential scanning calorimetry (MDSC). A TA Instruments TGA machine (Q5000 SA, Delaware, USA) equipped with Universal Analysis 2000 software (TA Instruments, Delaware, USA), was used to evaluate the residual water content within the films. The samples were weighed accurately (2–5 mg) and heated at 10 °C min^{-1} from 25 to 300 °C with a steady flow (50 mL min^{-1}) of dry nitrogen. Thermal transitions were analyzed for the films and pure starting materials on a TA Instruments DSC Q2000 (Delaware, USA) machine with modulated function (MDSC) enabled to ensure better detection of the glass transition (T_g) peak. About 3–5 mg of each sample was weighed in aluminium pans with lids pierced and heated from 25 to 220 °C (5 °C min^{-1}), cooled (10 °C min^{-1}) to 0 °C and heated back to 220 °C at a rate of 5 °C min^{-1}.

2.8. Microscopic examination

A Nicolet iN 10 IR microscope (Thermo Fisher Scientific, Loughborough, UK) and scanning electron microscope (SEM) (Hitachi SU8030 SEM (Berkshire, UK)) were used to map the film surface for uniform distribution and determine surface morphology respectively, as previously reported [48] and briefly summarized below. For the IR mapping, 2D and 3D images (maps) and corresponding IR spectra for the major peaks determined from the ATR-FTIR analyses were collected from random portions of the films' surfaces. In the case of SEM, samples were coated with chromium and images acquired using accelerated voltage and working distance of 20 kV and 15 mm respectively.

2.9. In vitro drug dissolution studies

The *in vitro* release of TM from the DL films (X2, B2) was evaluated using a specialized flow system that collects sample fractions automatically. The set up comprised a collector system (Gilson FC204, Middleton, USA) and SC100 immersion circulators (Thermo Fisher, Loughborough, UK) which were maintained at 37 °C and a peristaltic pump with multiple channels (Longer Pump BT100-1L, Hebei, China). This arrangement allowed all the samples to be analyzed for TM release simultaneously and also allowed continuous flow (50 μL min^{-1}) of STF over the film samples to ensure sink conditions throughout the experiment. This automated sampling technique at the given flow rate was set to mimic the tear turnover in the eye. STF was pumped into the chamber containing the sample from one end and flowed out of the chamber into the collector at the opposite end. At specific time intervals the STF in the sample collector was transferred into glass vials for HPLC analysis. The TM was analyzed following a previously reported method by Rodriguez and co-workers [58] on an Agilent Technologies 1200 HPLC instrument (Cheshire, UK) using a 15.0 × 0.46 cm Spherisorb S5 ODS1 column with 5 μm particle size as stationary phase. The mobile phase comprised methanol, water and trimethylamine (TEA) in a ratio of 80:20:0.2 respectively at a flow rate of 1 mL min^{-1} and detection wavelength set at 259 nm.

2.10. In vitro drug permeation using EpiCorneal™ tissue

Human cornea-like epithelial kit (Fig. S1), was procured from MatTek Corporation (MA, USA) and the tissues were immediately equilibrated to room temperature. The 6-well plates containing the EpiCorneal™ tissue samples were then incubated in a humidified incubator (37 °C; 5 % CO_2) overnight prior to performing the permeability experiments. To ensure the tissues were healthy and viable, they were visually examined under sterile conditions for the presence of any air bubbles at the interface of the agarose gel and the inserts. Once healthy tissues were confirmed, the assay medium (1 mL) was placed into each well of previously labelled sterile 6-well plates.

The protocol utilized a 24-well plate for every 3 tissues and the assay medium was used as permeability buffer at 37 °C. Using sterile technique, 0.3 mL of pre-warmed assay medium was placed into the wells of 6 × 24-well plates. The well plates were labelled as follows: the 3 left wells were labelled "pre-incubation" and the remaining wells as 0.5, 1.0, 1.5, 2.0, and 2.5 h. A set of 3 tissues were designated as negative controls (NC) and all the well plates were placed in the incubator for 30 min. For the permeation, an indirect method which involved first hydrating the film samples (F3, X2, B2) in the assay medium was employed, while TM eye drops were applied directly. Before application of the film samples, donor solution (100 μL) was transferred into wells containing EpiCorneal™ tissues. After equilibrating for 30 min, the cell culture inserts containing the EpiCorneal™ tissues were moved to the 0.5 h wells and treated with the film extracts (100 μL). Subsequently, the plates were put back in the incubator for another 30 min and the tissues were moved to the 1.0 h wells. The process was repeated for 1.5, 2.0, and 2.5 h of total elapsed time. The permeation samples collected at each time point were then analyzed for TM by HPLC and permeation flux (J) calculated with Eq. (5) below.

$$J = dQ/dt.1/A \quad (5)$$

where J is steady-state flux, dQ/dt is amount of drug (TM) permeated at time t and A is effective diffusion area.

2.11. Ex vivo drug permeation using porcine cornea

Ex vivo permeation of TM released from the optimized films (F3, X2, B2) was investigated with the help of the automated fraction collector system used for the *in vitro* drug dissolution studies using fresh porcine eyes. The eyes were collected from a local slaughterhouse based in Kent, UK and immediately transferred into a cooler containing cold Krebs-Ringer bicarbonate buffer, quickly transported to the laboratory, and used within 2 h of collection as previously reported [59]. The cornea was carefully detached, separated and washed with PBS (pH 7.4) maintained at a temperature of 37 °C. The separated cornea was subsequently placed on the diffusion cell between the donor and the receiver compartments and samples automatically collected at specified time intervals over 24 h. In the case of the bilayer films, the HA side loaded with TM was in direct contact with the cornea mucosa surface. The flow rate of the medium (STF) was maintained at 50 μL min^{-1} over the films and porcine cornea and into the collector with the entire system kept at 37 °C. The total surface area of cornea placed on top of the diffusion cells was 1.3 cm^2 with 0.6 cm^2 diffusion surface area. The collected samples (n = 3) were analyzed for TM using HPLC and permeation flux (J) values were calculated using Eq. (5).

2.12. Permeation correlation between porcine cornea and EpiCorneal™ tissues

The permeability of TM across the porcine cornea and EpiCorneal™

tissues was further investigated by plotting a correlation curve of EpiCorneal™ cumulative permeation against the porcine cumulative permeation for all samples and the linear regression (R^2) values obtained for each film were compared.

2.13. Tissue integrity, cytotoxicity and cell viability

Preliminary MTT tests investigated blank single polymer films. In addition, aliquots of the pure TM solutions were also evaluated at five different concentrations to determine any potential cytotoxicity related to the drug dose. Furthermore, blank and DL composite (HA/HPMC) films prepared from 1% w/v gels) were also assessed for % cell viability to indicate possible cytotoxicity caused by combination of the two polymers or upon drug incorporation. Finally, the selected optimized formulations (F3, X1, X2, B1, B2) were also assessed for potential cytotoxicity. After the permeation experiments, the EpiCorneal™ tissue inserts were transferred into 24 well plates pre-filled with 300 μL of 3-(4,5-dimethylthiazol-2-yl)-2,5-diphenyltetrazolium bromide (MTT) dissolved in PBS (pH 7.4). The plates were then incubated for 3 h, the liquid was gently removed from all wells and the cultures were extracted in 2 mL of acidified isopropanol for 2 h with gentle shaking at 120 rpm. Afterwards, 200 μL of the extract was transferred into 96 well plates and the absorbance of the purple-colored formazan formed was determined by a microtiter plate reader (Multiskan FC, Thermo Fisher Scientific, Loughborough, UK) at a wavelength of 520 nm. Percentage cell viability was calculated for each tissue relative to the mean of the negative control (NC) tissues using Eq. (6) below. For this study, untreated cells were used as NC (100 % viable) while 0.01 % w/v of Triton-X-100 treated cells were used as positive controls (PC).

Further *in vitro* cytotoxicity evaluation of the ocular films was conducted using HeLa cells supplied by the tissue culture laboratory of the University of Greenwich (Richardson Lab, School of Science, Grenville Building, University of Greenwich at Medway, Kent, UK). The cytotoxicity test was performed by indirect contact of the samples with the cells as previously reported [60]. Cells were cultured in Dulbecco's Modified Eagle's Medium containing 10 % fetal bovine serum and 1 % penicillin-streptomycin (Thermo Fisher Scientific, Loughborough, UK) until they reached 70–80 % confluence before being challenged with the film samples. Films were cut into small disks using a 6 mm punching device and sterilized under UV radiation for 24 h. The samples were then immersed in 1.5 mL of complete medium and placed in a Heracell 150i CO_2 incubator (Thermo Fisher Scientific, Dartford, UK) at 37 °C for 24 h. The resulting liquid mixture was filtered through a 0.2 μm filter and the filtrate collected. The cell suspension for the experiment was prepared at a concentration of 1×10^5 cells per mL and 100 μL of cell suspension transferred into designated wells of 96-well microtiter plates. The plates were left in the 37 °C incubator at 5 % (v/v) CO_2 for 24, 48 and 72 h and cell viability was determined by the MTT assay method. For each time point (24, 48 and 72 h), 10 μL of MTT reagent was added to each well including media only and controls and left in the incubator for an additional 4 h. The culture media was then completely aspirated from all wells and replaced with 100 μL of DMSO and the plates returned to the incubator for 30 min after which the absorbance was recorded at 520 nm by a microtiter plate reader. Each experiment was conducted in triplicates (n = 3) and the percentage cell viability was calculated using Eq. (6).

$$\text{Cell viability } (\%) = \frac{At - Ab}{Ac - Ab} \times 100 \tag{6}$$

At, *Ab* and *Ac* are the absorbance of test samples, blank (medium only) and NC (untreated cells) respectively.

2.14. Statistical analysis

All the quantitative data generated were analyzed with one-way analysis of variance (ANOVA) followed by Tukey's post-hoc test and *t*-test with *p* values below 0.05 considered significant. All the results were presented as the mean of 3 replicates (± standard deviation), unless otherwise specified.

3. Results and discussion

3.1. Synthesis and formulation optimization

In preparing the bilayer films, HPMC and composite (HA/HPMC) films were initially attempted as the erodible top layer. However, the presence of HPMC caused polymer disentanglement and coalesced with the pHEMA/PVP slurry indicated by opacity of the resulting bilayer films (Fig. 2a & b). The polymer disentanglement observed was attributed to weak polymer chain interactions in HPMC film matrices which are more easily disrupted than those of HA films when in contact with the pHEMA/PVP. Furthermore, Ali and colleagues showed high swelling of methacrylate-based hydrogels at basic pH, and this explains ingress of water in and out of the films depending on the hydrogel's pH [61]. This is interesting as HPMC showed higher pH values than HA [48]. In addition, the coalescing and subsequent loss of transparency could be attributed to hydrogen bonding interaction between carbonyl groups of PVP and the hydroxyl groups of HPMC as previously reported by Somashekarappa and co-workers [62]. Synthesis of the pHEMA/PVP hydrogel presented temperature related challenges associated with the chemical and thermal properties of HEMA. The polymerization reaction of HEMA required heating at 50 °C for 14 h because the reaction is initiated only when the entire solution reaches 50 °C in a slow endothermic process. However, once the system reaches 50 °C, there is only a small window of approximately 15 min before HEMA solidifies (loss of flowability), after which it was not possible to remove unreacted monomers. According to Huang and Yang [63], this was due to the high activation energy of HEMA which makes its crosslinking reaction more sensitive to temperature. The presence of initiator, catalyst (crosslinker) and small amount of PVP (4 %) was reported to have no effect on the activation energy and hence the temperature dependent solidification of HEMA.

As a result, the temperature conditions had to be tightly controlled to enable successful formation of the free-flowing hydrogel. To overcome the challenges presented by composite HA/HPMC films when pHEMA/PVP hydrogel was poured onto them, HA only matrix films were prepared in order to obtain better bilayer formulations. Furthermore, for direct comparison, the HA matrix was crosslinked using PEGDE in the presence of IT. During the first stage of crosslinking, there is interaction between the COOH groups of IT with the OH groups of HA to form ester bonds, with IT maintaining an acidic pH environment. Subsequently, the epoxide functional group of PEGDE forms ester and ether bonds with the COOH and OH groups of HA respectively [64–66].

3.2. Physical evaluation

3.2.1. Transparency

The spectral profiles of light transmittance through the crosslinked HA and pHEMA/PVP-HA bilayer films are shown in Fig. 3, while that for F3 has been previously reported [48]. Formulations X1 and B1 (blank films) showed optimum transparency after immediate assessment of the films (Fig. 2c & d). HA demonstrated its ability to form thin transparent films after crosslinking as well as being a stable erodible drug carrier in bilayer films with no major sign of pHEMA/PVP-HA interaction. Despite the transparent visual appearance of all the selected optimized films, the light transmission test revealed lower % transmittance for X1 (72–83 %) and X2 (68–79 %) (Fig. 3) with values slightly below the ideal 80 % in the visible light region (400–700 nm) required for optimum vision after application [27,50].

On the other hand, the bilayer films (B1 and B2) showed overall light transmittance values above 80 % indicating suitable transparency for ocular application. Finally, a visual examination for transparency was

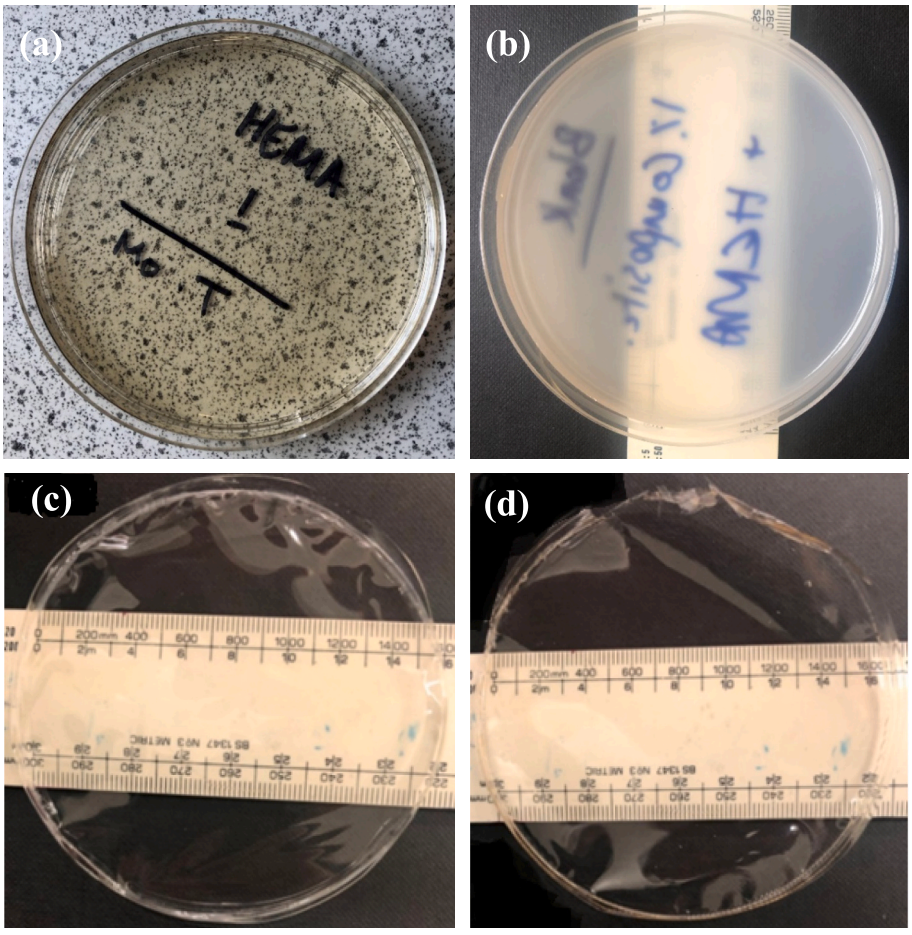

Fig. 2. Digital images of (a) synthesized pHEMA/PVP hydrogel; (b) after pouring on 1 % composite HA/HPMC film to produce bilayer film formulation showing the loss of transparency; (c) DL (HA crosslinked film – X2) and (d) DL (pHEMA/PVP-HA bilayer film - B2) showing optimum transparency from visual assessment soon after film formation.

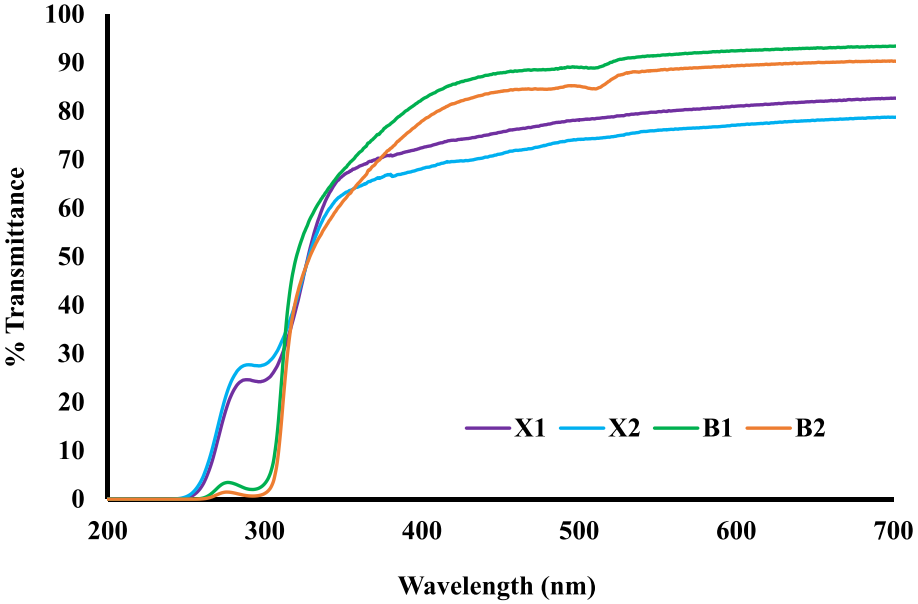

Fig. 3. UV–visible light transmission spectra of HA crosslinked and pHEMA/PVP-HA bilayer films.

undertaken for the four optimized formulations using 5 human volunteers. Interestingly, all participants scored 1 (completely transparent) for X1, X2, B1 and B2 films and complemented the analytical assessment using UV–visible spectrophotometry spectroscopy as slight variations in film transparency are not easy to detect by the naked human eyes. In addition to the light transmittance, another important functional

property for contact lenses that impact on their performance when applied, is the oxygen permeability and transmissibility which was not undertaken in the current study and will be required in future experiments.

3.2.2. Weight, thickness, surface pH and folding endurance

Table 4 shows the results for the weight, thickness, surface pH and folding endurance of the different film formulations. The bilayer (B1 and B2) films possessed higher values for weight and thickness compared to the single layer films (X1 and X2), simply due to the presence of two (HA and pHEMA/PVP) layers.

In addition, despite some increase in thickness values at higher polymer concentrations, the change observed was not statistically significant ($p > 0.05$). This was attributed to the presence of crosslinkers in X1 and X2 as well as the pHEMA/PVP layer for B1 and B2, which reduced the distance between the polymer chains resulting in a more compact film matrix. Interestingly, the thickness of similar crosslinked HA hydrogel films reported by Calles (2016) and Grimaudo (2018) were 157 (± 17) μm and 275 (± 66) μm respectively [25,26], which were higher than the maximum thickness value of 48 (± 8) μm observed for X2 in this study. Tightly bound polymer chains provide lower availability of unoccupied spaces for residual moisture which directly influences sample weight and other characteristics such as folding endurance and percentage elongation. The poor folding endurance performance for X1 and X2 confirms this evaluation (Table 3). Folding endurance is also directly influenced by the presence of plasticizer, in this case GLY. Assessment of surface pH revealed adequate values for all the formulations, ranging between 5.5 (± 0.02) and 6.8 (± 0.03) which is within accepted pH range for ocular delivery systems [67]. Therefore, X1, X2, B1 and B2 present suitable surface pH for topical administration on the ocular surface and are not expected to cause any irritation when applied.

3.3. Swelling capacity

Erodible single layer films prepared from 1 % HA gels showed maximum swelling capacity of 2497 ± 30 % as previously reported [48], which was deemed suitable. However, crosslinked HA formulations (X1 and X2) showed higher swelling profiles than erodible HA films and pHEMA/PVP-HA bilayer films (Fig. 4a) due to X1 and X2 containing two times the amount of HA. Further, the swelling capacity results for X1 and X2 were higher than similarly crosslinked HA films reported by Calles and co-workers [24,25], which can be explained by the presence of GLY in the HA films prepared in this study. Hydrophilic plasticizers such as GLY increase the specific volume between polymer chains [68] which allows easier ingress of water molecules with resultant increase in the rate of hydration and subsequently higher % swelling capacity.

The ability of X1 and X2 to absorb high amounts of water and maintain their swollen matrix structure without disintegrating is related to the presence of PEGDE crosslinker which holds the polymer chains tightly bound. Water present in hydrophilic films is classified as free (bulk) or bound water. The bound water is non-covalently associated to the polymer as illustrated in (Fig. 4b) and can be further divided into slightly and tightly bound water [69,70]. When a dry film is placed in an aqueous environment, the water initially binds to the polar, hydrophilic groups *via* hydrogen bonding resulting in primary bound water, which initiates matrix swelling. Once the matrix swells, hydrophobic groups become exposed to water and the excess water entering the swollen gel matrix then interacts with these hydrophobic groups to form secondary bound water [69,70]. Both the primary and secondary bound water together constitute what is referred to as total bound water [71,72]. The polymeric matrix continued to absorb water until it reached equilibrium where maximum swelling was achieved (within 40 min in the case of X1 and X2). The water which fills the pores and spaces within the hydrogel once equilibrium is reached, is referred to as free or bulk water [73]. The amount of water at the polymer surfaces can play a vital role in biocompatibility and drug release from hydrogels [74].

The swelling of bilayer (B1 and B2) films showed similar profiles to the single layer erodible 1 % w/v HA films previously reported [48]. This is not surprising, since the HA layer of the bilayer films was largely responsible for swelling and subsequent erosion of B1 and B2. Furthermore, the DL films (X2 and B2) showed no major variation in swelling profiles when compared to their corresponding blank (X1 and B1) films. This is to be expected, since the bottom layer of the bilayer films were similar to soft contact lenses which are designed not to disintegrate but rather supposed to maintain their structural integrity when in contact with fluids.

Table 4
Weight, thickness, surface pH and folding endurance results of DL formulations (n = 3, ± SD).

Film	Weight (mg)	Thickness (μm)	Surface pH	Folding endurance
X1	83 ± 5	44 ± 5	6.80 ± 0.03	217 ± 21
X2	81 ± 4	48 ± 8	6.70 ± 0.04	224 ± 23
B1	125 ± 6	66 ± 21	5.50 ± 0.02	>300
B2	127 ± 6	72 ± 13	5.60 ± 0.01	>300

3.4. Tensile properties

The results for tensile properties are summarized in Table 5. Tensile strength and elastic modulus values of crosslinked HA (X1 and X2) films were significantly higher ($p < 0.05$) while the % elongation values were significantly lower ($p < 0.05$) than the bilayer (B1 and B2) films. The results demonstrate better mechanical strength of X1 and X2, while B1 and B2 revealed better flexibility and completely in line with the results from folding endurance as shown in Table 4. Furthermore, the tensile strength and elastic modulus values for X1, X2, B1 and B2 films were significantly higher ($p < 0.05$) than those obtained for non-crosslinked single layer HA films [48].

Further, % elongation values for X1 and X2 were significantly lower ($p < 0.05$) than B1 and B2. This was attributed to the compact polymer matrix structure caused by crosslinking of HA as well as by the higher total polymer content in those films resulting in a denser matrix. Elongation at break, which represents flexibility, is directly influenced by the amount of GLY which acts to plasticize the films. Both X1 and X2 contained lower amounts of plasticizer relative to the total polymer content compared to B1 and B2 (Table 1). Low amounts of plasticizer, high total polymer concentration and strong crosslinking result in a reduction of polymer chain mobility and decreased % elongation as well as folding endurance. Khan and co-workers reported that presence of plasticizers in the system increase the free volume between the polymeric chains, allowing them to slide past each other and subsequently produced appropriate flexibility and consequent decrease in tensile strength and elastic modulus [75]. However, the low % elongation for X1 and X2 suggests these two formulations may be brittle, though physical handling and the folding endurance values showed them to be relatively flexible but tough. The flexibility and pliability could be improved by first soaking in water briefly prior to being applied, which is common with SCLs currently on the market.

3.5. In vitro mucoadhesion

Table 6 shows the results from *in vitro* mucoadhesive assessment of the films. The bilayer (B1 and B2) films showed significantly higher ($p < 0.05$) stickiness (PAF) compared to X1 and X2, while the differences in TWA and cohesiveness results were not statistically significant ($p > 0.05$) for the two sets of formulations. During measurement for the stickiness for bilayer films, the pHEMA/PVP layer was in contact with the adhesive tape stuck to the probe while the HA layer made direct contact with the gelatin substrate. This was done to simulate real life application as the HA layer containing the TM was intended to be

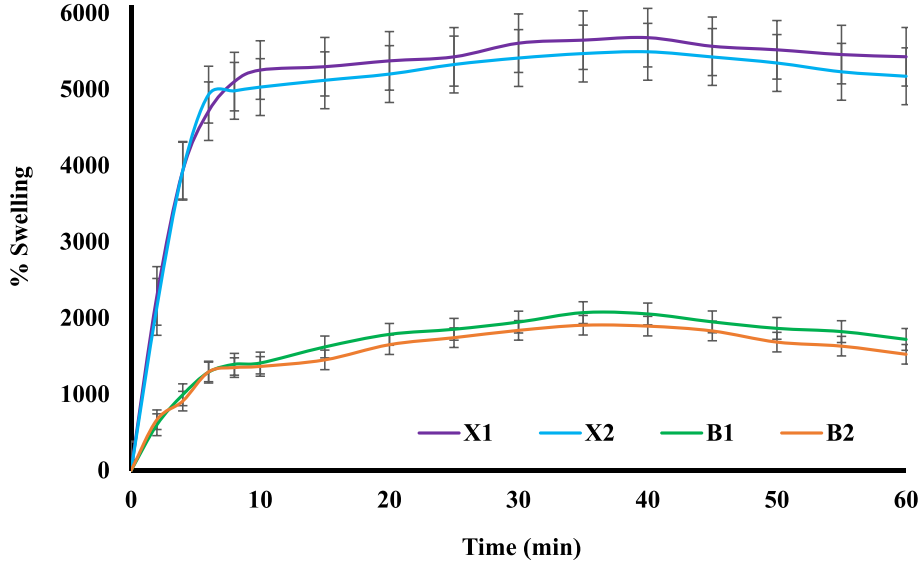

Fig. 4. Swelling capacity profiles of formulations X1, X2, B1 and B2 (n = 2, ± SD).

Table 5
Tensile strength, elastic modulus and percentage elongation values of cross-linked and bilayer films calculated from stress/strain curve (n = 3, ± SD).

Films	Tensile strength (Nmm^{-2})	Elastic modulus (mPa)	Elongation (%)
X1	1629.2 ± 311.2	1766.2 ± 51.2	3.4 ± 0.4
X2	1539.8 ± 145.3	1777.2 ± 113.9	3.7 ± 0.4
B1	170.0 ± 40.1	67.3 ± 14.7	53.3 ± 12.2
B2	176.0 ± 31.6	54.5 ± 8.1	70.6 ± 11.9

Table 6
Mucoadhesion (PAF, TWA and cohesiveness) profiles for the selected optimized formulations (n = 3, ± SD).

Films	PAF (N)	TWA (N/s)	Cohesiveness (mm)
X1	4.9 ± 1.0	1.6 ± 0.3	10.5 ± 0.3
X2	5.6 ± 3.0	1.3 ± 0.8	9.0 ± 2.2
B1	11.0 ± 1.5	5.0 ± 1.6	9.4 ± 6.6
B2	8.8 ± 2.4	3.1 ± 0.7	10.2 ± 1.4

applied directly onto the ocular mucosa (cornea). The major adhesive mechanisms at play were attributed to van der Waals forces as well as weak hydrogen bonding between COOH groups of HA and mucin present in the STF [76].

However, given the higher PAF values observed for the bilayer films compared to the other HA films, it is possible that there was a further contribution from PVP present in the pHEMA/PVP layer through secondary hydrogen bonding between PVPs carbonyl functional groups and the gelatin surface once the films had been hydrated. Furthermore, the HA layer for the B1 and B2 films contained lower amounts of HA (prepared from 1 % w/v gels) resulting in thinner films compared to X1 and X2 prepared from 2 % crosslinked HA gels. The thinner films were more easily hydrated in the presence of STF which is an essential step in the initial stages of adhesion. This allowed easier interpenetration between the polymeric chains of HA and mucin, in line with the diffusion theory of mucoadhesion. The cohesiveness values of X1, X2, B1 and B2 were generally higher than the non-crosslinked single layer HA (F3) based films reported previously [48]. Enhanced cohesiveness and stickiness, together with slight delay of erosion observed during swelling of B1 and B2 could contribute to increased retention time of these formulations on the ocular surface.

3.6. Sterilization effect

Ocular formulations are required to be sterile to avoid the potential for infection when applied and sterilization by UV radiation is a simple and cost-effective method that can preserve sample biocompatibility. Short-wave UV irradiation with wavelength ranging from 200 to 280 nm causes disruption of DNA-based pairing resulting in inactivation of bacteria, viruses and protozoa [77]. However, sterilization methods such as radiation can cause deleterious effects on certain functional physical and chemical properties of formulations which can negatively impact on their performance *in vivo* [78,79]. Therefore, tensile and mucoadhesion properties were used to determine the potential effects of UV radiation on the optimized TM loaded (DL) films.

The tensile and adhesive results obtained for the DL-loaded films (F3, X2, B2) after sterilization (Table 7) were compared with results of non-sterilized films presented in Tables 5 and 6. Sterilization by UV radiation showed no significant effect ($p > 0.05$) on physical and mechanical properties of the films prepared in this study.

Tensile strength (Nmm^{-2}) value of F3 decreased from 49.7 (± 5.4) to 45.8 (± 1.2). Similar changes were observed for X2 and B2 with tensile strength value of X2 increasing from 1539.8 (± 145.3) to 1786.2 (± 123.2) Nmm^{-2} while B2 decreased from 176.0 (± 31.6) to 171.1 (± 7.4) Nmm^{-2}. A similar pattern was observed in % elongation where X2 increased from 3.7 (± 0.4) to 5.2 % (± 1.2) while B2 value decreased

Table 7
Effects of sterilization on tensile and mucoadhesive properties of the films (n = 3, ± SD).

Tensile properties			
Film	Tensile Strength (Nmm^{-2}) ± SD	Elastic Modulus (mPa) ± SD	Elongation (%) ± SD
F3	45.8 ± 1.2	3.5 ± 1.4	49.9 ± 1.2
X2	1786.2 ± 123.2	1592.7 ± 276.5	5.2 ± 1.2
B2	171.1 ± 7.4	42.4 ± 24.0	43.0 ± 8.8

Mucoadhesion properties			
Film	PAF (N) ± SD	TWA (N/s) ± SD	Cohesiveness (mm) ± SD
F3	3.8 ± 1.6	6.4 ± 0.8	5.1 ± 0.8
X2	6.2 ± 4.0	1.6 ± 0.9	10.2 ± 0.6
B2	8.6 ± 3.3	3.0 ± 0.9	9.8 ± 1.8

from 70.6 % (± 11.9) to 43.0 % (± 8.8). The slight variations observed were attributed to exposure to air over the 24 h period which could have caused changes in moisture content of the films. Loss or gain of water can alter the mechanical properties of films due to water's well-known plasticizing action [80]. The moisture differences could also be due to preparing a new batch of films for assessing the effect of sterilization on the mechanical properties.

Similar to the tensile properties, there was no marked effect of UV sterilization on the mucoadhesive properties of the films with insignificant differences ($p > 0.05$) observed. In composite HA/HPMC films (F3), PAF values before and after sterilization were 3.8 N (± 0.4) and 3.8 N (± 1.6) respectively, while the cohesiveness reduced from 5.2 (± 0.4) to 5.1 (± 0.8). In X2, all mucoadhesion properties (PAF, TWA and cohesiveness) demonstrated slight increases after sterilization, while B2 showed slight decreases but these changes were not significant. The fluctuation in mucoadhesion results suggests that the dissimilarities observed after sterilization may not be attributed fully to UV radiation, but more related to changes in physicochemical properties of the

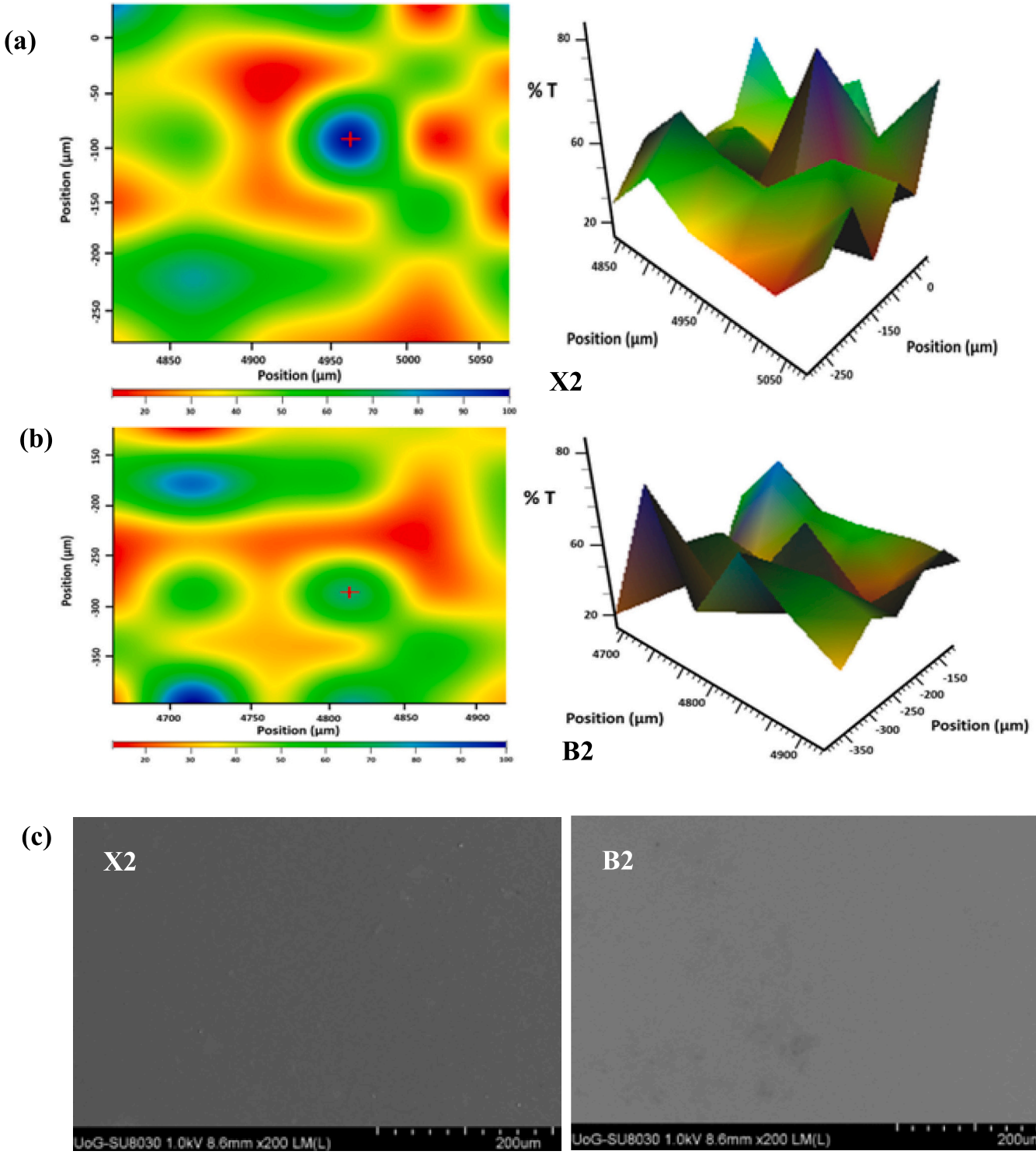

Fig. 5. 3D (right) and 2D IR maps of (a) X2 and (b) B2 illustrating the distribution of TM across the films (c) SEM micrographs of X2 and B2.

prepared batch such as residual moisture content.

3.7. Analytical characterization

3.7.1. ATR-FTIR spectroscopy

Fig. S2 shows the ATR-FTIR spectra of crosslinked HA and bilayer films which showed structural domination of HA in the bilayer films and no major shift in principal peaks of HA upon crosslinking in X1 and X2. The presence of TM in the drug loaded formulations was confirmed by the small shoulder peak around 1580 cm^{-1} related to bending of –NH groups, with most of the other major TM peaks suppressed due to the significantly higher amounts of HA. Further details of the other expected peaks can be found in the corresponding supplementary data section.

3.7.2. XRD

The physical form (crystalline or amorphous) of the films were determined by XRD and the diffractograms are shown in Fig. S3 and indicate no differences between the blank and TM loaded films. All the films showed halo diffraction patterns which confirmed the amorphous nature of all the films which implies the pure TM which exhibited sharp crystalline peaks was molecularly dispersed within the HA film matrix. Such molecular dispersion can be useful in topical drug delivery, as amorphous drugs show better drug release behavior compared to the corresponding crystalline forms.

3.7.3. Thermal analyses

The residual water content in X1, X2, B1 and B2 films was determined by TGA and the results are presented in Table S1 with further discussion in the relevant section of the supplementary data. Furthermore, physical form, stability and interactions between the various excipients in the films were examined using MDSC and the results are shown in Fig. S4. All films can be characterized as amorphous due to absence of sharp endothermic peak which is typically associated with melting peak of crystalline materials and confirmed the XRD results described above.

3.8. Microscopic examination

Two microscopic approaches were used to analyze surface morphology as well as drug distribution within the polymeric matrix of the TM-loaded films. The IR microscope images confirmed that the HA crosslinked and pHEMA/PVP-HA bilayer films showed suitable drug distribution over the entire surface with translucent strands representing functional groups of TM observed in the IR maps for both X2 and B2. The maps obtained from analyzing the principal IR peaks of TM in both formulations (Fig. 5a & b respectively) displayed green, yellow and amber colors indicating 30–70 % density for TM. The blue circles represent areas on the film surface with >80 % density of TM and corresponds to small regions of the drug molecules entrapped within a fixed space in the film matrix. This was more distinctive in crosslinked HA films (X2) compared to the bilayer film (B2). Homogeneous distribution of drug across the entire film matrix is essential to assure uniform drug release and subsequent penetration across the whole cornea surface rather than being restricted to a small area. Though the data obtained shows the presence of drug across the film surface, the uniformity of drug distribution could be further improved, for example by increasing the duration of stirring the gels before being cast and dried.

SEM images (Fig. 5c) for X2 and B2 showed smooth surface morphology compared to single layer non-crosslinked HA films (F3) previously reported [48], where pockets of polymer entanglement were observed on their surfaces. This is due to a more compact matrix structure due to crosslinking of the polymer chains, as well as the longer gelation process required for the crosslinking reaction to come to completion. Furthermore, addition of pHEMA/PVP slurry at 50 °C and potential hydrogen bonding between the hydroxyl groups of pHEMA and HA eliminates any undissolved or entangled polymer chains which resulted in the smooth surface of the bilayer films. Overall, the SEM results confirmed the IR mapping profiles and shows that they will be suitable for easy application without potential for irritation, though other analytical techniques such as atomic force microscopy will provide more definitive information about surface roughness/smoothness.

3.9. In vitro drug release

Release of TM from X2 and B2 films was assessed with a calibration curve (Fig. S5) and the cumulative drug release profiles are shown in Fig. 6. The release was slower from X2 which achieved maximum percentage drug release (27.4 %) while B2 reached maximum cumulative drug (57.5 %) within 8 h and both profiles closely mirrored the corresponding swelling profiles, shown in Fig. 4.

This is interesting because single layer erodible films (F3) prepared from 1 % w/v composite HA/HPMC gels previously reported [48], released 71.6 % of TM. The slower rate of TM release from X2 is hypothesized to be due to entrapped drug molecules within the strongly bound polymer network of the crosslinked film (higher total polymer content) and provided more viscous resistance to drug diffusion out of the swollen matrix. On the contrary, TM was only available in the thin HA layer of the bilayer films and since this HA layer was not crosslinked, it was more erodible compared to X2. However, the cumulative release was lower than that of 1 % w/v HA film which was likely due to some of the drug molecules on the lower surface of HA layer attaching to the sticky pHEMA/PVP layer, thus reducing the total amount of drug available for release once the HA layer was fully swollen.

Therefore, the objective of prolonged drug release was achieved due to crosslinking the drug carrier *i.e.*, HA polymer matrix and should avoid the need for frequent administration. Calles and co-workers investigated TM release from non-transparent crosslinked HA ocular inserts designed to be applied to the eye's cul de sac [24]. Their study demonstrated rapid initial release over the first 4 h followed by continuous release of TM over 24 h. However, these ocular inserts were limited by their poor transparency (opaque), high thickness and poor flexibility which presents a risk of irritation. In a related study, Grimaudo and co-workers [81] investigated the release profiles of cyclosporine from crosslinked HA films. Interestingly, their films achieved maximum cumulative release of cyclosporine within 8 h or less compared to the crosslinked HA films in the current study and this could be attributed to the differences in drug properties and possibly due to different grades of HA. Lee and colleagues [23] investigated TM release profiles from single layer pHEMA contact lenses and showed maximum percentage drug release within 4 h which was significantly faster than both X2 and B2. This illustrates the critical role of HA as the drug carrier layer in B2, demonstrating its ability to provide sustained drug release as well as increasing retention time, both contributing to prolonged delivery of TM to the eyes.

3.10. Drug permeation studies

3.10.1. In vitro permeation using EpiCorneal™ tissue

Fig. 7a shows the permeation profiles of TM released from the DL films through the model EpiCorneal™ tissue while the permeation flux (J) of TM from the formulations are shown in Table 8. The most prescribed dosage form for glaucoma is eye drops, therefore 0.5 % w/v TM eye drops were used as control in the permeation studies and compared with the DL films.

The reconstructed human cornea-like epithelial tissue was prepared in inserts with a porous membrane through which the nutrients passed to the cells. The reconstructed tissue possesses a non-keratinized epithelium that simulated the cornea epithelium with progressively stratified but not cornified cells. Among the films tested, the highest cumulative permeation and permeation flux (J) within 150 min was observed for F3 with maximum cumulative permeation of 64.8 μg cm^{-2} and permeation flux (J) of 107.9 (± 1.2) μg cm^{-2} h^{-1} while the lowest

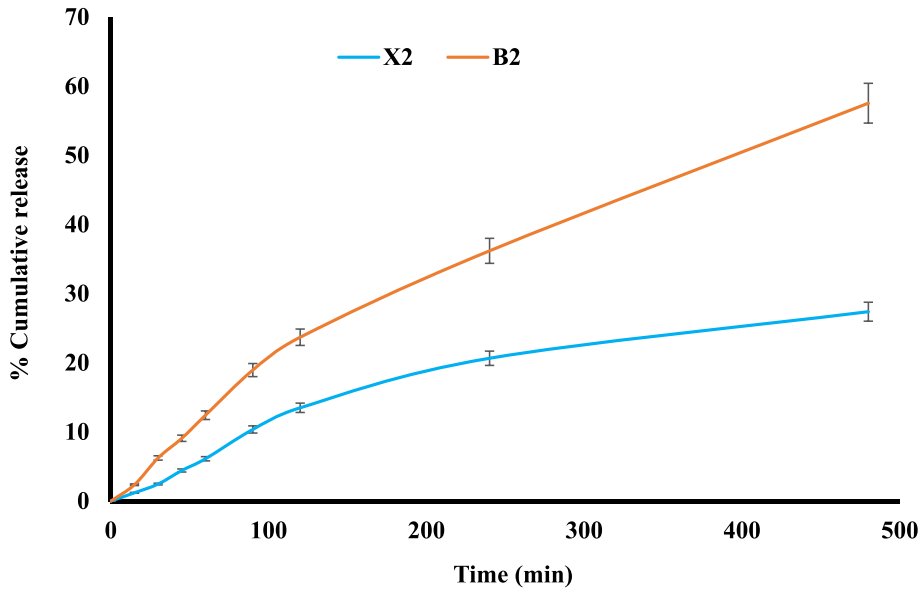

Fig. 6. Percentage cumulative drug release from X2 and B2 films (n = 2, ± SD).

values were observed for B2 with cumulative permeation and permeation flux (J) of 22.5 μg cm^{-2} and 37.6 (± 1.2) μg cm^{-2} h^{-1} respectively. Interestingly, the eye drop showed the fastest permeation rate and also achieved maximum permeation within 120. This shows rapid release and permeation of the TM with little control compared to the films and confirms the main drawback of eye drops and hence the need for developing polymeric films to prolong the drug release, subsequent permeation and bioavailability *in vivo*.

EpiCorneal™ tissue construct is a recent development by the manufacturer and there is no published research discussing the permeability of TM or similar drugs using this particular tissue model. EpiOcular™ was used by Kandarova and co-workers [46] for eye irritation test and by Ko and colleagues [47] for ocular toxicity assessment. Katoh and colleagues [82] used an alternative reconstructed human corneal epithelial model (LabCyte), which was again used for evaluation of eye irritancy. The only published article related to EpiCorneal™ is by Kaluzhny and colleagues [41], who assessed very low concentrations (0.005 % w/v) of Latanoprost solutions, but the data was not comparable to this study.

3.10.2. *Ex vivo* drug permeation using porcine tissue

The cumulative permeation curves of TM released from the films through porcine cornea are shown in Fig. 7b and the permeation flux (J) of the formulations are shown in Table 8. The highest cumulative permeation and permeation flux (J) was shown by F3 with values of 1702.1 μgcm^{-2} and 1045.1 (± 0.2) μgcm^{-2} h^{-1} respectively within 24 h while the lowest values were obtained for B2 with maximum values of 375.3 μgcm^{-2} and 312.12 (± 0.5) μgcm^{-2} h^{-1} respectively within 16 h. Lower permeation for B2 can be explained by the swelling profiles, which can affect the drug diffusion from the swollen gel. More specifically, drug diffusion can be explained by Fick's equation, which correlates the drug's flux with its concentration gradient, surface area and membrane thickness. Therefore, the diffusion of the drug is affected by the structure, polymer composition, the water content of the films, and the nature and size of the drug.

Crosslinking HA (X2) or combining with pHEMA/PVP as bilayer (B2) produced a tighter polymer network, which resulted in improved mechanical properties and subsequently a slower drug release rate reflecting on the number of drug molecules available for penetrating across the porcine cornea compared to the non-crosslinked erodible equivalent (F3). The permeation profiles observed in our study were similar to that reported by Reichl and colleagues [83], using excised porcine cornea. Although pig eye is the most identical to that of humans, many studies have reported *ex vivo* data utilizing rabbit eye with drug permeability across porcine cornea reported to be three to nine times lower than rabbit cornea [84]. This is interesting because the permeation flux (J) obtained in this study were all higher than those reported by Abdelbary and co-workers [85] where the highest permeation flux (J) across excised rabbit cornea was about 2.4 μg cm^{-2} h^{-1}. However, ketoconazole was the model drug in their study, and chemical properties of the drug play a key role in its permeation flux. For instance, TM (log P = 1.44) is a hydrophilic drug while ketoconazole (log P = 4.35) is very hydrophobic. Hydrophobic drugs show poor topical ocular permeation due to presence of tear film (mainly composed of water) and stroma layer of cornea (90 % of cornea's thickness) which is the main barrier to lipophilic drugs. Limited data available in literature relating to TM permeation across porcine cornea makes this data difficult to compare with other studies. However, the data obtained in this study illustrates the high potential of these formulations to achieve high and sustained permeation of TM through porcine cornea.

The permeation results from EpiCorneal™ support the *ex vivo* results confirming higher release and permeation for F3 which are erodible films. Higher cumulative permeation (μgcm^{-2}) and permeation flux (J, μgcm^{-2} h^{-1}) observed for porcine cornea experiment is attributed to the fact that the *ex vivo* permeation study was conducted for 24 h while permeation assessment using EpiCorneal™ was only 150 min long in line with the manufacturer instructions. This is considered a limitation as the novel approaches for ocular drug delivery are intended to prolong the release of the drug, and 150 min permeation time does not provide an accurate estimation of drug permeation in real life applications. Therefore, use of the *ex vivo* porcine cornea seems to be a more appropriate model to simulate human ocular permeation while the EpiCorneal™ tissue culture model will be useful for rapid initial screening of various formulations during product development.

The *in vitro* and *ex vivo* permeation data were further plotted to determine any correlation between them and representative correlation between the cumulative permeation curve of TM in the films using porcine cornea and EpiCorneal™ reconstructed 3D tissue is shown in Fig. S6 of supplementary data. The results showed a positive correlation between permeation using EpiCorneal™ tissue and porcine cornea for all formulations tested.

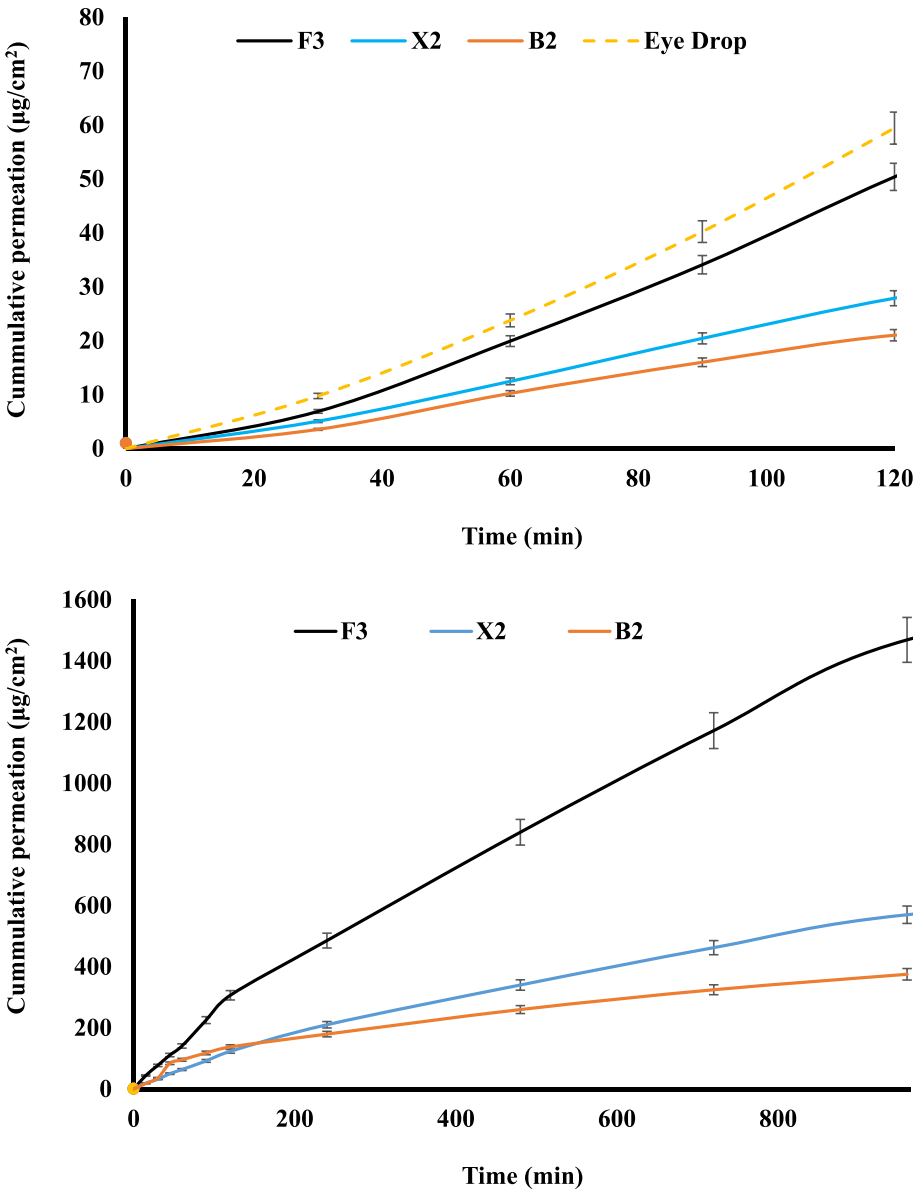

Fig. 7. (a) *In vitro* cumulative permeation curves of TM released from the optimized DL films compared with a commercial eye drop preparation using EpiCorneal™ tissue (n = 2, ± SD); Maximum permeation of eye drop was within 120 min, while F3, X2 and B2 showed a more controlled and prolonged permeation behavior up to 150 min as shown in Fig. S6. (b) *ex vivo* cumulative permeation curves of optimized films using porcine cornea tissue (n = 2, ± SD). F3 showed the highest permeation among all formulations tested, while F3 and X2 demonstrated more prolonged permeation than B2 as shown in the extended plot shown in Fig. S6.

Table 8
Permeation flux (J) of TM released from the DL films through the model EpiCorneal™ tissue and porcine cornea (n = 2, ± SD).

Film sample	Flux (J) (µg cm^{-2} h^{-1})	
	EpiCorneal™	Porcine cornea
F3	107.9 ± 1.2	1418.4 ± 0.2
X2	55.2 ± 0.6	549.0 ± 0.3
B2	37.6 ± 1.2	312.1 ± 0.5
Eye drop	99.1 ± 0.2	–

3.11. Cytotoxicity and cell viability

Assessment of cytotoxicity is vital for any materials that come into contact with the ocular surface. The polymers used in this study are currently being used in many pharmaceutical formulations and are listed as GRAS by the FDA. Both HA and HPMC are currently added to commercially available eye drops as thickening agents, while pHEMA-based contact lenses are still available for vision correction. However, the combination of different polymers and excipients with the drug and any potential interactions during film formation at different temperatures may produce harmful by-products. Therefore, cytotoxicity assessment by measuring cell viability using MTT assay was used to confirm safety of the prepared formulations. The assay investigates the reduction of yellow MTT to an insoluble purple formazan by enzymes (succinate dehydrogenase) found in the mitochondria of viable cells [86–88]. A major drawback encountered while assessing the tissue integrity was insufficient sample volume available which subsequently caused single sampling for technical replicate MTT measurements. Hela cells are one of the most widely used human cell lines in biological testing with over 70,000 studies published involving the use of HeLa cells. This is because HeLa cells grow easily and unusually rapidly, doubling cellular count in only 24 h, as long as they are fed the right mix of nutrients, making them ideal cell lines for large scale testing.

The results from MTT assay are illustrated in Fig. S7 (a, b) and Fig. 8a for the pure drug aliquots and selected optimized films respectively, compared with the controls. The results showed high % cell viability for the pure drug, blank and TM-loaded films over 72 h.

The accepted % cell viability is expected to be >70 % according to the ISO specification [60] and all the formulations showed cell viability values above 70 %, confirming their suitability for direct application to the ocular surface for up to 72 h.

Data obtained after 24 h showed the % viability of X2 and B1 at 67.3 % and 68.9 %, which are slightly lower than the expected value. However, these two values increased to 76.6 % and 77.5 % after 48 h. The lower % viability observed during the first 24 h is suspected to be due to potential disturbance upon initial handling of those specific wells. In addition, cell viability of X1 and B2 which had the same polymer composition as X2 and B1, respectively, were above 70 % within the same period which confirms that the lower values observed in X2 and B1 are not due to cytotoxicity of the formulations but due to experimental variations. To further confirm the biocompatibility of the formulated films, the viability of the EpiCorneal™ after the permeation experiments, were assessed using MTT and the % viability results are shown in Fig. 8b. The results showed that the films can be considered safe as the percentage cell viability values were all >70 % after 48 h and complements the results in Fig. 8a. However, the MTT assay only provides indication of biocompatibility in terms of cell viability and does not provide information about the potential for the films to cause acute local irritation in the eyes when applied. This can be achieved with the help of the OECD approved Draize test using albino rabbits' eyes (*in vivo*) as detailed in the OECD Test Guideline No. 405 [89] (OECD Test guideline

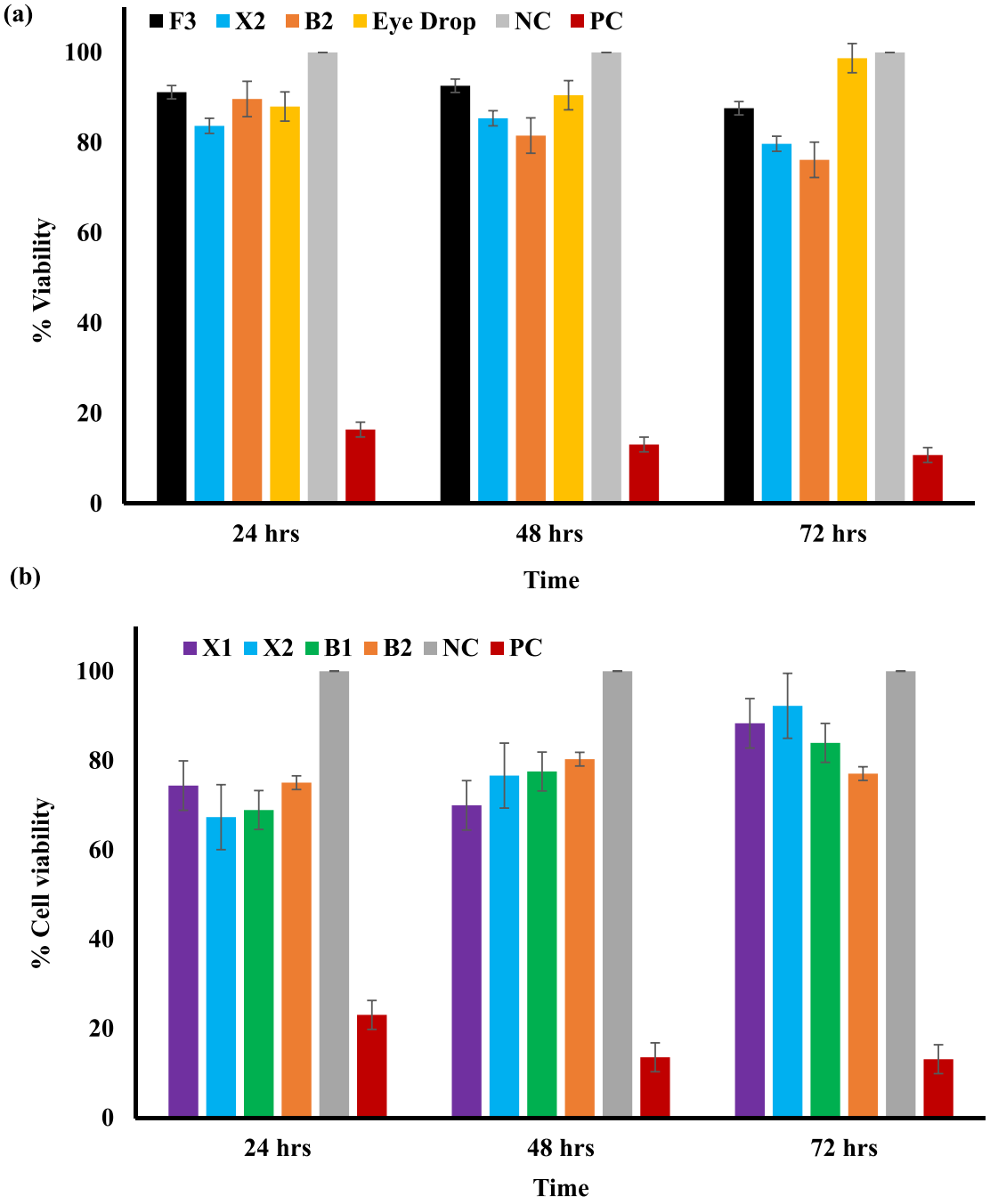

Fig. 8. (a) Cell viability of HeLa cells after exposure to the extracts of X1, X2, B1 and B2; for 24, 48 and 72 h (n = 6, ± SD); (b) viability of treated EpiCorneal™ tissues after permeation studies (NC = negative control, PC = positive control).

405) as well as using *in vitro* tissue culture models [46,47].

4. Conclusion

Both single layer crosslinked HA (X1, X2) and bilayer pHEMA/PVP-HA (B1, B2) films demonstrated adequate mechanical and physico-chemical characteristics for potential ocular drug delivery. Crosslinking HA and incorporation of the pHEMA/PVP layer enhanced tensile strength, mucoadhesion and surface morphology of the films which will improve the handling and drug retention time on the ocular surface. However, the swelling and *in vitro* drug dissolution studies revealed better performance of the crosslinked HA films compared to the bilayer films with the former showing higher swelling capacity and more controlled drug release profiles. ATR-FTIR and IR mapping results confirmed the presence of drug across the entire film surface with no major drug-polymer interaction which shows that any interactions between polymer and drug was due to weak hydrogen bonding and van de Waals forces, while DSC and XRD results revealed amorphization of the drug in the film matrices. The prolonged release, amorphization of the drug in the polymer matrix and enhanced retention time, all demonstrate promising characteristics of these films as potential topical ocular drug delivery platforms. This is the first study comparing permeation TM released from both HA matrix films and HA-based bilayer films through EpiCorneal™ (*in vitro*) and pig cornea (*ex vivo*) for potential treatment of glaucoma. The permeability results revealed relatively similar permeation profiles for X2 and B2, however, F3 showed significantly higher cumulative permeation and permeation flux than X2 and B2. The foregoing observation suggests the possibility of predicting experimental *in vivo* trends for permeation of TM *via* formulations prepared in this study through porcine cornea since a good linear correlation between *in vitro* and *ex vivo* experiments was achieved. MTT assay showed biocompatibility of all the films tested, which was further confirmed by evaluation of EpiCorneal™ tissues previously used for drug permeation. The possibility of directly loading TM into HA based matrices in combination with pHEMA based contact lens (bilayer) will help overcome a major limitation in their use for drug delivery by avoiding the need to soak them in drug solution to achieve appropriate loading. However, the current study is limited by the lack of *in vivo* experiments to determine therapeutic efficacy, therefore, future work involving preclinical animal glaucoma model will be required to validate the films' effectiveness to treat patients with glaucoma as well as confirming absence of irritation (Draize test) when applied. Finally, for purposes of using as contact lens, the oxygen permeability and transmissibility will need to be measured to confirm their suitability for regular use.

Funding

This research did not receive any specific grant from funding agencies in the public, commercial, or not-for-profit sectors.

CRediT authorship contribution statement

Mohammad Tighsazzadeh: Writing – review & editing, Visualization, Validation, Methodology, Investigation, Formal analysis, Data curation. **Joshua Boateng:** Writing – review & editing, Writing – original draft, Supervision, Resources, Project administration, Funding acquisition, Conceptualization.

Declaration of competing interest

The authors declare that they have no known competing financial interests or personal relationships that could have appeared to influence the work reported in this paper.

Appendix A. Supplementary data

Supplementary data to this article can be found online at https://doi.org/10.1016/j.ijbiomac.2024.129496.

References

[1] A.P. Marques, J. Ramke, J. Cairns, T. Butt, H.B. Faal, H. Taylor, I. Jone, N. Congdon, A. Bastawaite, T. Braithwaite, M. Jovic, S. Resnikoff, A. Nandakuma, P.T. Khaw, R.R.A. Bourne, I. Gordon, K. Frick, M.J. Burton, Estimating the global cost of vision impairment and its major causes: protocol for a systematic review, BMJ Open 10 (2020) e036689.
[2] D. Huang, Y.S. Chen, I.D. Rupenthal, Overcoming ocular drug delivery barriers through the use of physical forces, Adv. Drug Deliv. Rev. 126 (2018) 96–112.
[3] M.S. Khan, P.R. Ravi, S.I. Mir, P.S. Rawat, Optimization and *in vivo* evaluation of triamcinolone acetonide loaded *in situ* gel prepared using reacted tamarind seed xyloglucan and kappa-carrageenan for ocular delivery, Int. J. Biol. Macromol. 233 (2023) 123533.
[4] Q. Bao, B. Newman, Y. Wang, S. Choi, D.J. Burgess, In vitro and ex vivo correlation of drug release from ophthalmic ointments, J. Control. Release 276 (2018) 93–101.
[5] A.F. Hanafy, A.M. Abdalla, T.K. Guda, K.E. Gabr, P.G. Royall, A. Alqurshi, Ocular anti-inflammatory activity of prednisolone acetate loaded chitosan-deoxycholate self-assembled nanoparticles, Int. J. Nanomedicine 14 (2019) 3679–3689.
[6] T. Lajunen, R. Nurmi, L. Kontturi, L. Viitala, M. Yliperttula, L. Murtomäki, A. Urtti, Light activated liposomes: functionality and prospects in ocular drug delivery, J. Control. Release 244 (2016) 157–166.
[7] R. Kumar, V.R. Sinha, Preparation and optimization of voriconazole microemulsion for ocular delivery, Colloids Surf. B: Biointerfaces 117 (2014) 82–88.
[8] X. Wang, S. Wang, Y. Zhang, Advance of the application of nano-controlled release system in ophthalmic drug delivery, Drug Deliv. 23 (2016) 2897–2901.
[9] A. Mandal, R. Bisht, I.D. Rupenthal, A.K. Mitra, Polymeric micelles for ocular drug delivery: from structural frameworks to recent preclinical studies, J. Control. Release 248 (2017) 96–116.
[10] S. Lin, C. Ge, D. Wang, Q. Xie, B. Wu, J. Wang, K. Nan, Q. Zheng, W. Chen, Overcoming the anatomical and physiological barriers in topical eye surface medication using a peptide-decorated polymeric micelle, ACS Appl. Mater. Interfaces 11 (2019) 39603–39612.
[11] J.H. Jung, B. Chiang, H.E. Grossniklaus, M.R. Prausnitz, Ocular drug delivery targeted by iontophoresis in the suprachoroidal space using a microneedle, J. Control. Release 277 (2018) 14–22.
[12] S.H. Park, D.H. Jo, C.S. Cho, K. Lee, J.H. Kim, S. Ryu, C. Joo, J.H. Kim, W. Ryu, Depthwise-controlled scleral insertion of microneedles for drug delivery to the back of the eye, Eur. J. Pharm. Biopharm. 133 (2018) 31–41.
[13] F.J. Navarro-Gil, F. Huete-Toral, C.O. Domínguez-Godínez, G. Carracedo, A. Crooke, Contact lenses loaded with melatonin analogs: a promising therapeutic tool against dry eye disease, J. Clin. Med. 11 (2022) 3483.
[14] H. Abdelkader, B. Pierscionek, R.G. Alany, Novel in situ gelling ocular films for the opioid growth factor-receptor antagonist naltrexone hydrochloride: fabrication, mechanical properties, mucoadhesion, tolerability and stability studies, Int. J. Pharm. 477 (2014) 631–642.
[15] E. Terreni, P. Chetoni, S. Burgalassi, S. Tampucci, E. Zucchetti, E. Chipala, R. G. Alany, A.A. Al-Kinani, D. Monti, A hybrid ocular delivery system of cyclosporine-a comprising nanomicelle-laden polymeric inserts with improved efficacy and tolerability, Biomater. Sci. 9 (2021) 8235–8248.
[16] J.M. González-Méijome, L. Madalena, L.-A. Antonio, B.A. José, A.P. Manuel, F.R., Miguel Refractive index and equilibrium water content of conventional and silicone hydrogel contact lenses, Ophthamol. Physiol. Optics. 26 (1) (2006) 57–64.
[17] T.-H. Tsung, Y.-H. Chen, D.-W. Lu, Updates on biodegradable formulations for ocular drug delivery, Pharmaceutics 15 (3) (2023) 734.
[18] S.R. Chethana, M.G. Ahmed, Hydrogel contact lens for extended delivery of an anti-biotic in combination with anti-inflammatory drug for ophthalmic application, Asian J. Biomed. Pharm. Sci. 5 (46) (2015) 16–21.
[19] R. Li, X. Guan, X. Lin, P. Guan, X. Zhang, Z. Rao, L. Du, J. Zhao, J. Rong, J. Zhao, Poly(2-hydroxyethyl methacrylate)/β-cyclodextrin-hyaluronan contact lens with tear protein adsorption resistance and sustained drug delivery for ophthalmic diseases, Acta Biomater. 110 (2020) 105–118.
[20] F.A. Maulvi, T.G. Soni, D.O. Shah, A review on therapeutic contact lenses for ocular drug delivery, Drug Deliv. 7544 (2016) 1–10.
[21] V. Singh, S.S. Bushetti, A.A. Raju, R. Ahmad, M. Singh, M. Ajmal, Polymeric ocular hydrogels and ophthalmic inserts for controlled release of timolol maleate, J. Pharm. Bioallied Sci. 3 (2) (2011) 280–285.
[22] C. Torres-Luna, N. Hu, A. Koolivand, X. Fan, Y. Zhu, R. Domszy, J. Yang, A. Yang, N.S. Wang, Effect of a cationic surfactant on microemulsion globules and drug release from hydrogel contact lenses, Pharmaceutics 11 (6) (2019) 262.
[23] D. Lee, S. Cho, H.S. Park, I. Kwon, Ocular drug delivery through pHEMA-hydrogel contact lenses co-loaded with lipophilic vitamins, Sci. Rep. 6 (2016) 34194.
[24] J.A. Calles, L.I. Tártara, A. Lopez-García, Y. Diebold, S.D. Palma, E.M. Vallés, Novel bioadhesive hyaluronan–itaconic acid crosslinked films for ocular therapy, Int. J. Pharm. 455 (1–2) (2013) 48–56.
[25] J.A. Calles, A. Lopez-Garcia, E.M. Valles, S.D. Palm, Y. Diebold, Preliminary characterisation of dexamethasone-loaded cross-linked hyaluronic acid films for topical ocular therapy, Int. J. Pharm. 509 (1–2) (2016) 237–243.

[26] S. Casey-Power, R. Ryan, G. Behl, P. McLoughlin, M.E. Byrne, L. Fitzhenry, Hyaluronic acid: its versatile use in ocular drug delivery with a specific focus on hyaluronic acid-based polyelectrolyte complexes, Pharmaceutics 14 (2022) 1479.
[27] M. Korogiannaki, G. Guidi, L. Jones, H. Sheardown, Timolol maleate release from hyaluronic acid-containing model silicone hydrogel contact lens materials, J. Biomater. Appl. 30 (3) (2015) 361–376.
[28] A.R. Desai, F.A. Maulvi, M.M. Pandya, K.M. Ranch, B.A. Vyas, S.A. Shah, D. O. Shah, Co-delivery of timolol and hyaluronic acid from semi-circular ring-implanted contact lenses for the treatment of glaucoma: in vitro and in vivo evaluation, Aust. J. Biol. Sci. 6 (2018) 1580–1591.
[29] R.V. Nair, S. Shefrin, A. Suresh, K.R. Anoop, S.C. Nair, Sustained release timolol maleate loaded ocusert based on biopolymer composite, Int. J. Biol. Macromol. 110 (2018) 308–317.
[30] G.R. Silva, A.P.R. Almeida, G.M. Fernandes-Cunha, B.F.M. Castro, L.C. Vieira, G. O. Fulgêncio, A. Silva-Cunha, S.L. Fialho, Safety and in vivo release of fluconazole-loaded implants in rabbits' eyes, J. Drug Deliv. Sci. Technol. 35 (2016) 323–326.
[31] A.V. Dumitrescu, J. Bertram, L.R. Olson, J.K. Jens, N.M. Ellinwood, Y.H. Kwon, E. Lavik, M.H. Kuehn, In-vivo characterization of sustained release timolol microspheres, Invest. Ophthalmol. Vis. Sci. 51 (13) (2010) 3166.
[32] T. Fujihara, T. Murakami, H. Fujita, M. Nakamura, K. Nakata, Improvement of corneal barrier function by the P2Y(2) agonist INS365 in a rat dry eye model, Invest. Ophthalmol. Vis. Sci. 42 (2001) 96–100.
[33] W. Chen, X. Zhang, J. Zhang, J. Chen, S. Wang, Q. Wang, J. Qu, A murine model of dry eye induced by an intelligently controlled environmental system, Invest. Ophthalmol. Vis. Sci. 49 (2008) 1386–1391.
[34] D. Dursun, M. Wang, D. Monroy, D.Q. Li, B.L. Lokeshwar, M.E. Stern, S. C. Pflugfelder, A mouse model of keratoconjunctivitis sicca, Invest. Ophthalmol. Vis. Sci. 43 (2002) 632–638.
[35] S.A. McLaughlin, A.H. Brightman, L.C. Helper, N.D. Primm, M.G. Brown, S. Greeley, Effect of removal of lacrimal and third eyelid glands on Schirmer tear test results in cats, J. Am. Vet. Med. Assoc. 193 (1988) 820–822.
[36] C.P. Moore, J.B. McHugh, J.G. Thorne, T.E. Phillips, Effect of cyclosporine on conjunctival mucin in a canine keratoconjunctivitis sicca model, Invest. Ophthalmol. Vis. Sci. 42 (2001) 653–659.
[37] S.J. Hicks, A.P. Corfield, R.L. Kaswan, S. Hirsh, M. Stern, J. Bara, S.D. Carrington, Biochemical analysis of ocular surface mucin abnormalities in dry eye: the canine model, J. Exp. Eye Res. 67 (1998) 709–718.
[38] Y. Dang, S. Waxman, C. Wang, R.T. Loewen, M. Sun, N.A. Loewen, A porcine ex vivo model of pigmentary glaucoma, Sci. Rep. 8 (2018) 5468.
[39] K.Y. Chan, P. Cho, M. Boost, Corneal epithelial cell viability of an ex vivo porcine eye model, J. Clin. Exp. Opt. 97 (4) (2014) 337–340.
[40] E.P. Choy, P. Cho, I.F. Benzie, C.K. Choy, Dry eye and blink rate simulation with a pig eye model, J. Opt. Vis. Sci. 85 (2008) 129–134.
[41] S. Pescina, P. Govoni, A. Potenza, C. Padula, P. Santi, S. Nicoli, Development of a convenient ex vivo model for the study of the transcorneal permeation of drugs: histological and permeability evaluation, J. Pharm. Sci. 104 (2015) 63–71.
[42] P. Agarwal, I.D. Rupenthal, In vitro and ex vivo corneal penetration and absorption models, Drug Deliv. Transl. Res. 6 (2016) 634–647.
[43] Y. Kaluzhny, M.W. Kinuthia, T. Truong, A.M. Lapointe, P. Hayden, M. Klausner, New human organotypic corneal tissue model for ophthalmic drug delivery studies, Invest. Ophthalmol. Vis. Sci. 59 (2018) 2880–2898.
[44] J.S. Boateng, O. Okeke, Evaluation of clay-functionalized wafers and films for nicotine replacement therapy via buccal mucosa, Pharmaceutics 11 (3) (2019) 104.
[45] J.S. Boateng, J.C. Mitchell, H.V. Pawar, I. Ayensu, Functional characterisation and permeation studies of lyophilised thiolated chitosan xerogels for buccal delivery of insulin, Protein Pept. Lett. 21 (11) (2014) 1163–1175.
[46] H. Kandarova, S. Letasiova, E. Adriaens, R. Guest, J.A. Willoughby, A. Drzewiecka, K. Gruszka, N. Alépée, S. Verstraelen, A.R. Van Rompay, CON4EI: EpiOcular™ eye irritation test (EpiOcular™ EIT) for hazard identification and labelling of eye irritating chemicals, Toxicol. in Vitro 49 (2018) 21–33.
[47] K.Y. Ko, M.H. Hong, T.S. Kim, K.T. Nam, G.Y. Lee, J.S. Yi, I.Y. Ahn, J.H. Kim, J. K. Lee, Ezrin as a complementary marker in ocular toxicity assessment using a three-dimensional reconstructed human corneal-like epithelium model, EpiOcular™, J. Pharmacol. Toxicol. Methods 92 (2018) 24–33.
[48] M. Tighsazzadeh, J.C. Mitchell, J.S. Boateng, Development and evaluation of performance characteristics of timolol-loaded composite ocular films as potential delivery platforms for treatment of glaucoma, Int. J. Pharm. 566 (2019) 111–125.
[49] O. Grytsenko, L. Dulebova, O. Suberlyak, V. Skorokhoda, E. Spišák, I. Gajdoš, Features of structure and properties of pHEMA-gr-PVP block copolymers, obtained in the presence of Fe^{2+}, Materials (Basel) 13 (20) (2020) 4580.
[50] A. Valente, A. Pimenta, B. Saramago, A.P. Serro, Use of a surfactant (CAC) for controlling the release of ophthalmic drugs from hydrogels for contact lenses, in: Conference Proceedings: Materiais 2015 – VII International Materials Symposium and XVII Conference Sociedade Portuguesa dos Materiais, 2015.
[51] S. Fujimura, T. Nagasawa, M. Kawamura, T. Sato, T. Sato, The sterilization effect against *Staphyloccocus aureus* and *Pseudomonas aeruginosa* on the contact lens using the ultraviolet C irradiation, J. Infect. Pub. Health 13 (2) (2020) 350.
[52] J.S. Boateng, A.M. Popescu, Composite bi-layered erodible films for potential ocular drug delivery, Colloids Surf. B: Biointerfaces 145 (2) (2016) 353–361.
[53] R. Fuentes, E. Fernandez, I. Pascual, C. Garcia, UV-visible transmittance of silicone-hydrogel contact lenses measured with a fiber optic spectrometer, Proc. SPIE-Int. Soc. Opt. Eng. 8785 (2013) 8785AZ-1.
[54] K.R.N. Priya, S. Bhattacharyya, B.P. Ramesh, Formulation and evaluation of erodible ocular films of valacyclovir hydrochloride, Dhaka Univ. J. Pharm. Sci. 13 (1) (2014) 75–81.
[55] J.S. Boateng, F. Hafezi, A.G. Tabriz, D. Douroumis, 3D printed dressings loaded with human epidermal growth factor for potential chronic wound healing applications, J. Drug Deliv. Sci. Technol. 86 (2023) 104684.
[56] F. Hafezi, N. Scoutaris, D. Douroumis, J.S. Boateng, 3D-printed chitosan dressing crosslinked with genipin for potential healing of chronic wounds, Int. J. Pharm. 560 (2019) 406–415.
[57] M. Yamaguchi, K. Ueda, A. Isowaki, A. Ohtori, H. Takeuchi, N. Ohguro, K. Tojo, Mucoadhesive properties of chitosan-coated ophthalmic lipid emulsion containing indomethacin in tear fluid, Biol. Pharm. Bull. 32 (7) (2009) 1266–1271.
[58] I. Rodriguez, J.A. Vazquez, L. Pastrana, V.V. Khutoryanskiy, Enhancement and inhibition effects on the corneal permeability of timolol maleate: polymers, cyclodextrins and chelating agents, Int. J. Pharm. 529 (2017) 168–177.
[59] S. Khan, V. Trivedi, J.S. Boateng, Functional physico-chemical, ex vivo permeation and cell viability characterization of omeprazole loaded buccal films for pediatric drug delivery, Int. J. Pharm. 500 (1–2) (2016) 217–226.
[60] A. Ahmed, J.S. Boateng, Calcium alginate-based antimicrobial film dressings for potential healing of infected foot ulcers, Ther. Deliv. 9 (3) (2018) 185–204.
[61] L. Ali, M. Ahmad, M. Usman, Evaluation of cross-linked hydroxypropyl methylcellulos graft-methacrylic acid copolymer as extended release oral drug carrier, Cellul. Chem. Technol. 49 (2) (2015) 143–151.
[62] H. Somashekarappa, Y. Prakash, K. Hemalatha, T. Demappa, R. Somashekar, Preparation and characterization of HPMC/PVP blend films plasticized with sorbitol, Indian J. Mater. Sci. 2013 (2013) 307514 (7 pages).
[63] Y. Huang, J. Yang, Novel Colloidal Forming of Ceramics, Springer Science & Business Media, Beijing, China, 2020.
[64] J.C. Imperiale, G.B. Acosta, A. Sosnik, Polymer-based carriers for ophthalmic drug delivery, J. Control. Release 285 (2018) 106–141.
[65] S. Brännström, M. Finnveden, M. Johansson, M. Martinelle, E. Malmström, Itaconate based polyesters: selectivity and performance of esterification catalysts, Eur. Polym. J. 103 (2018) 370–377.
[66] S. Khunmanee, Y. Jeong, H. Park, Crosslinking method of hyaluronic acid-based hydrogel for biomedical applications, J. Tissue Eng. 8 (2017) 2041731417726464.
[67] S. Ahmed, M.M. Amin, S. Sayed, Ocular drug delivery: a comprehensive review, AAPS PharmSciTech 24 (2023) 66.
[68] J.S. Boateng, H.N.E. Stevens, G.M. Eccleston, A.D. Auffret, M.J. Humphrey, K. H. Matthews, Development and mechanical characterization of solvent-cast polymeric films as potential drug delivery systems to mucosal surfaces, Drug Dev. Ind. Pharm. 35 (8) (2009) 986–996.
[69] W. Li, F. Xue, R. Cheng, States of water in partially swollen poly(vinyl alcohol) hydrogels, Polymer 46 (25) (2005) 12026–12031.
[70] A.D.H. Al-Shohani, Hydrogel Formulations for Ophthalmic Delivery (PhD Thesis), University College London, 2016, pp. 47–63.
[71] T. Wang, S. Gunasekaran, States of water in chitosan-PVA hydrogel, J. Appl. Polym. Sci. 101 (5) (2006) 3227–3232.
[72] B.L. Dargaville, D.W. Hutmacher, Water as the often neglected medium at the interface between materials and biology, Nat. Commun. 13 (2022) 4222.
[73] H. Hatakeyama, T. Hatakeyama, Interaction between water and hydrophilic polymers, Thermochim. Acta 308 (1–2) (1998) 3–22.
[74] K. Hayakawa, M. Kawaguchi, T. Kato, Protective colloidal effects of hydroxypropyl methyl cellulose on the stability of silicone oil emulsions, Langmuir 13 (23) (1997) 6069–6073.
[75] S. Khan, J.S. Boateng, V. Trivedi, J.C. Mitchell, Formulation, characterisation and stabilisation of buccal films for paediatric drug delivery of omeprazole, AAPS PharmSciTech 16 (4) (2015) 500–510.
[76] J.-M. Gu, J.R. Robinson, S.-H.S. Leung, Binding of acrylic polymers to mucin/epithelial surfaces: structure-property relationships, Crit. Rev. Ther. Drug Carrier Syst. 5 (1988) 21–67.
[77] A.S. Hoffman, Hydrogels for biomedical applications, Adv. Drug Deliv. Rev. 64 (2012) 18–23.
[78] R.P. Rastogi, R.A. Kumar, M.B. Tyagi, R.P. Sinha, Molecular mechanisms of ultraviolet radiation-induced DNA damage and repair, J. Nucleic Acids 16 (2010) 1–32.
[79] R. Galante, A.S. Oliveira, A. Topete, D. Ghisleni, M. Braga, T.J.A. Pinto, R. Colac, A. P. Serro, Drug-eluting silicone hydrogel for therapeutic contact lenses: impact of sterilization methods on the system performance, Colloids Surf. B: Biointerfaces 161 (2018) 537–546.
[80] C.C. Yeh, C.N. Chen, Y.T. Li, C.W. Chang, M.Y. Cheng, H.I. Chang, The effect of polymer molecular weight and UV radiation on physical properties and bioactivities of PCL films, Cell. Polym. 30 (5) (2011) 261–275.
[81] M.A. Grimaudo, S. Nicoli, P. Santi, A. Concheiro, C. Alvarez-Lorenzo, Cyclosporine-loaded cross-linked inserts of sodium hyaluronan and hydroxypropyl-β-cyclodextrin for ocular administration, Carbohydr. Polym. 201 (2018) 308–316.
[82] M. Katoh, F. Hamajima, T. Ogasawara, K. Hata, Establishment of a new in vitro test method for evaluation of eye irritancy using a reconstructed human corneal epithelial model, LabCyte cornea-model, Toxicol. in Vitro 27 (7) (2013) 2184–2192.
[83] S. Reichl, J. Bednarz, C.C. Müller-Goymann, Human corneal equivalent as cell culture model for in vitro drug permeation studies, Br. J. Ophthalmol. 88 (4) (2004) 560–565.
[84] S. Pescina, P. Govoni, A. Potenza, C. Padula, P. Santi, S. Nicoli, Development of a convenient ex vivo model for the study of the transcorneal permeation of drugs: histological and permeability evaluation, J. Pharm. Sci. 104 (1) (2015) 63–71.
[85] G.A. Abdelbary, M.M. Amin, M.Y. Zakaria, Ocular ketoconazole-loaded proniosomal gels: formulation, ex vivo corneal permeation and in vivo studies, Drug Deliv. 24 (1) (2017) 309–319.

[86] O.C. Okeke, J.S. Boateng, Composite HPMC and sodium alginate based buccal formulations for nicotine replacement therapy, Int. J. Biol. Macromol. 91 (2016) 31–44.
[87] Cell viability assays, in: T.L. Riss, R.A. Moravec, A.L. Niles, S. Duellman, H. A. Benink, T.J. Worzella, L. Minor, S. Markossian, A. Grossman, K. Brimacombe, et al. (Eds.), Assay Guidance Manual, Eli Lilly & Company and the National Center for Advancing Translational Sciences, Bethesda (MD), 2013, pp. 1–31.
[88] W. Zeng, Q. Li, T. Wan, C. Liu, W. Pan, Z. Wu, G. Zhang, J. Pan, M. Qin, Y. Lin, C. Wu, Y. Xu, Hyaluronic acid-coated niosomes facilitate tacrolimus ocular delivery: mucoadhesion, precorneal retention, aqueous humour pharmacokinetics, and trans-corneal permeability, Colloids Surf. B: Biointerfaces 141 (3) (2016) 28–35.
[89] OECD/OCDE 405 © OECD, OECD guideline for the testing of chemicals for acute eye irritation/corrosion. https://www.oecd-ilibrary.org/deliver/9789264185333-en.pdf?itemId=/content/publication/9789264185333-en&mimeType=pdf, 2023. (Accessed 21 December 2023).